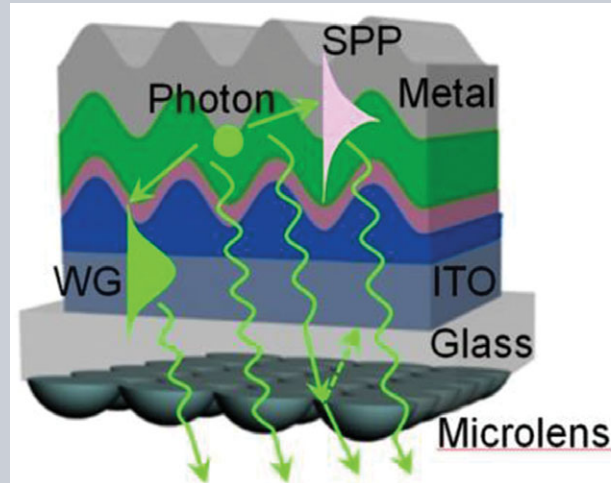


The demonstration of high efficiency and color tunability has brought organic light-emitting devices (OLEDs) into the lighting and display market. High efficiency is one of the key issues for their commercial applications, for which much effort has been devoted to developing novel materials and device structures. It is well known that around 80% of the generated photons are trapped in OLED structure, so that there is still the greatest scope for significant improvements in its efficiency. This has driven the research towards the integration of micro/nano patterns into device structures that benefit from their abilities in manipulating the generation and propagation of photons. Micro/nano patterns with random or periodic morphologies have demonstrated their effect on the outcoupling of the trapped photons within the device. Moreover, the emitting properties other than the light extraction could be manipulated by introducing the micro/nano patterns. This article reviews the recent progresses in improving the light extraction and manipulating the emission properties of the OLEDs through the introduction of the micro/nano patterns by various fabrication strategies. The light manipulation of the micro/nano patterns in organic

photovoltaics is briefly discussed considering its similar working principle and fabrication strategies to that of the OLEDs.



Light manipulation in organic light-emitting devices by integrating micro/nano patterns

Jing Feng, Yue-Feng Liu, Yan-Gang Bi, and Hong-Bo Sun*

1. Introduction

Intense academic research and substantial commercial efforts on organic light-emitting devices (OLEDs) have improved their promising applications in displays as well as for solid-state lightings [1–7]. The key characteristics of the OLEDs are their self-emitting property, wide viewing angle, high luminous efficiency associated with low power consumption, high contrast and fast switching speed. Considerable efforts have been made to improve OLED efficiency, because it is one of the most important requirements for the practical and commercial applications. However, very low light extraction efficiency is one of the main bottlenecks for its high efficiency. Around 80% of internally generated photons is trapped in form of waveguide (WG) modes in indium-tin-oxide (ITO) anode and organic layers (ITO/organic mode), and in surface plasmon-polariton (SPP) mode associated with the metallic cathode/organic interface, and also trapped in the substrate due to the total internal reflection at the glass/air interface (substrate mode) [8, 9]. The overall power lost even reaches to ~ 95% for the inorganic LEDs due to higher refractive index of inorganic semiconductors [10, 11]. Considering the significant power loss, it's therefore not surprising that the works on the light manipulation in the OLEDs is mainly focused on the improving of the light extraction by internal or external

structure modification, which has been an active area of research over recent years.

The substrate mode can be extracted by introducing a surface modification on the back side of the glass substrate, for example, attaching a commercial microlens array or a light extraction film [12–18]. However, it is more challenging to achieve the extraction of the power loss due to the light waveguiding in the ITO/organic layer or lost to SPP mode at the electrode surface without deteriorating the device performance, because a modification of the internal structure inside the device is required. Various techniques have been proposed to improve the light extraction by internal device structure modification with non-patterned or patterned profile. Using a non-patterned low refractive index layer as host for the emitters [19] would result in an improved outcoupling of the WG modes in the ITO/organic layers. On the other hand, a non-patterned high refractive index layer as substrate [20–22], and scattering particle with high refractive index embedded film as substrate [23, 24] or inserted between the transparent electrode and the glass substrate [24, 25] has demonstrated their effect on reducing the light trapping in the ITO/organic layers. No extra structuring or special optical elements is required for the simple and low-cost non-patterned strategy, except that light trapped in SPP mode at the metallic cathode/organic interface cannot be outcoupled by this method.

Micro/nano patterns with random or periodic morphologies have demonstrated their effect on the extraction of the trapped modes within the device [26–45]. Introducing a micro/nano pattern onto the metallic electrode/organic interface to provide an additional momentum to couple the SPP modes into light is especially crucial for recovering the power lost to the associated SPP modes [46–48]. Fabrication of the micro/nano patterns requires the simple and low cost manufacturing. The scope of this article is to review ongoing efforts to realize the enhanced light extraction of the OLEDs by using the micro/nano patterns. The effect of the micro/nano pattern-induced light manipulation on the light extraction, light emitting properties and the fabrication technique of the micro/nano patterns in the OLEDs will be discussed. The micro/nano patterns are widely used in organic photovoltaics (OPVs) for light harvesting [49–52], which will be roughly discussed in this review article because of its similar light manipulation principle and fabrication strategies to that of the OLEDs.

2. Fundamental principle of micro/nano patterns on light manipulation

2.1. Power lost in OLEDs

The operation of the OLEDs involves charge injection and transport followed by radiative recombination of injected opposite charges to generate light inside the device. The external quantum efficiency (EQE) η_{ext} is defined as the ratio of the total number of photons emitted by the OLED into the viewing direction to the number of electrons injected into the OLED device [9]:

$$\eta_{ext} = \gamma \eta_r q_{eff} \eta_{out} = \eta_{int} \eta_{out} \quad (1)$$

where γ represents the charge carrier balance, η_r is the fraction of the excitons that is allowed to decay radiatively by spin statistics, and q_{eff} is the effective quantum efficiency specifying the fraction of spin allowed excited states that actually decay by emitting a photon. It can be split into an internal quantum efficiency η_{int} times the external coupling efficiency η_{out} (the fraction of the total number of photons that can escape the device). Statistically, 75% of injected charges are in the three-fold degenerate triplet state, while only 25% are in the singlet excited state, except that the ratio of the singlet exciton formation for polymer materials could be higher [53–55]. The triplet states of the fluorescent materials do not emit light, so that the η_{int} is limited to 25% for the singlet–harvesting fluorescent organic materials. Much effort has been devoted to develop electrophosphorescent materials, which have significant spin-orbit coupling [56,57]. Nearly 100% η_{int} of the OLEDs can be achieved by means of harvesting both singlet and triplet excitation states using phosphorescent emitting materials [58–60], as well as a balanced carrier injection and recombination and suppressed non-radiative exciton quenching. On the other hand, using thermally activated up-conversion

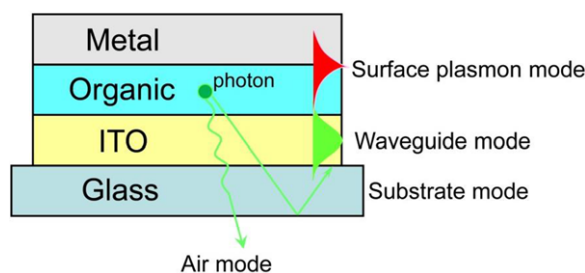


Figure 1 Schematic diagram of optical modes in OLEDs.

of triplet into singlet states to give thermally activated delayed fluorescence provide a new triplet harvesting method without the need of the phosphorescent materials [61–63]. Consequently, the η_{ext} of the OLEDs is no longer limited by the emission efficiency of the organic material itself, but the light extraction efficiency of their device structure. Considering the 25% extraction efficiency of the conventional OLED device, the maximum EQE is limited to less than 25% despite achieving nearly 100% internal quantum efficiency.

The typical device structure of a conventional OLED consists of glass substrate coated with transparent conducting oxide as anode, an organic light-emitting layer sandwiched between hole-transport and electron-transport layers and a metal cathode is deposited on the top of the device. Frequently, the anode of the OLED consists of ITO with high transparency and good electrical conductivity. The refractive index of the glass substrate ($n \approx 1.5$) is usually lower than that of the organic ($n \approx 1.7$) and ITO ($n \approx 2.0$) layers, which results in the power lost in form of ITO/organic mode trapped inside the organic and ITO layers due to the total internal reflection. The total internal reflection also occurs at the glass/air interface and contributes to the power lost to the substrate mode. Therefore, the light is emitted into four types of modes: air mode where the light escapes the substrate, and trapped modes of substrate, ITO/organic (WG) and SPP modes as shown in Fig. 1. Several analytical models have been employed to quantitatively calculate the power lost to the four types of modes, for example, ray-optics model [64], wave optical methods [9] and radiative transport model [65]. The power lost within the device depends on the structure parameters such as the thickness of the ITO and organic layers, the location of the emission zone and the dipole orientation [66–68]. Most of the results up to now have predicted light extraction efficiency of around 25% for bottom-emitting OLEDs [9,64,66,69]. As an example, the contribution of the air, substrate, SPP and ITO/organic modes for a prototypical Alq₃-based OLED stack are 15.3%, 24.3%, 43.7% and 11.0%, respectively [9].

2.2. SPP loss in OLEDs

SPPs are guided electromagnetic surface modes with transverse magnetic (TM) polarization that occur at the interface

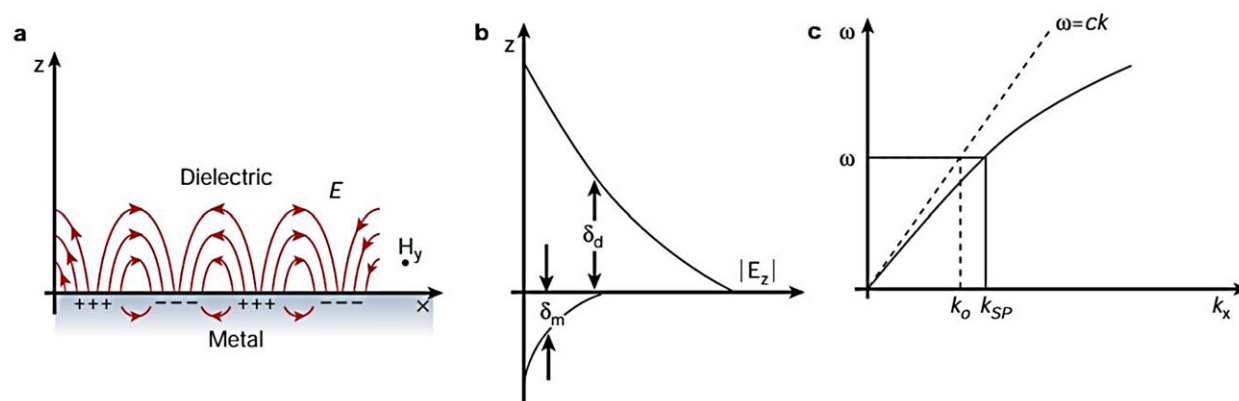


Figure 2 SPPs at the interface between a metal and a dielectric material have a combined electromagnetic wave and surface charge character as shown in (a). This combined character also leads to the field component perpendicular to the surface being enhanced near the surface and decaying exponentially with distance away from it (b). The dispersion curve for a SPP mode shows the momentum mismatch in (c). δ_m and δ_d is decay length of the field into the metal and the dielectric medium above the metal, respectively (with permission of Ref. [73]. Copyright 2003 Nature Publishing Group).

between a metal and a dielectric [70–74]. An analytical solution could be obtained as $k_{spp} = k_0(\epsilon_m\epsilon_d/(\epsilon_m + \epsilon_d))^{1/2}$ for SPP resonance at the metal/dielectric interface as shown in Fig. 2a, where ϵ_m and ϵ_d are the permittivity of the metal and dielectric, respectively. Metallic layers are usually employed in OLEDs as electrodes for the charge injection, while SPP modes are supported at the metallic electrode/organic interface. Excitons formed by the injected opposite charges may decay by coupling to the SPPs. SPPs have electromagnetic fields that decay exponentially into both the bounding metal and dielectric media (Fig. 2b). They are nonradiative in nature on a planar interface, because they possess a greater momentum than free space photons of the same frequency (Fig. 2c). Therefore, for a conventional planar OLEDs structure, the energy coupled from excitons to SPP modes cannot couple out from the device, and it is, in general, lost as heat. It was reported that the SPP loss is up to about 40% in typical planar small-molecule based OLEDs as shown in Fig. 3 [9, 47]. It is noted that the SPP loss is dramatically less than 10% for the polymer-based OLEDs. This is because the SPP loss depends strongly on the orientation of the dipole moment associated with the excitons [75]. The dipole moments of the polymer deposited by spin casting process lie in the plane of the film. The electric fields associated with the SPP mode are predominantly normal to the surface so that the dipole moments lying in the plane minimize coupling between the excitons in the polymer and SPP modes [53–55]. While in case of the small molecules deposited by thermal evaporation, the excitons have no preferred orientation, so that their coupling with the SPP modes is much stronger. It should be noted that there are some small-molecule emitters exhibiting preferential alignment of the emitting dipoles, such as predominantly horizontal orientation to the substrate, which would reduce the coupling to SPPs [9]. Preferentially horizontal orientation for several small molecules by thermal evaporation has been demonstrated, which enhance the out-coupling by around 45% [76–81]. The orientation of the dipole orientation for the amorphous film of the evaporated

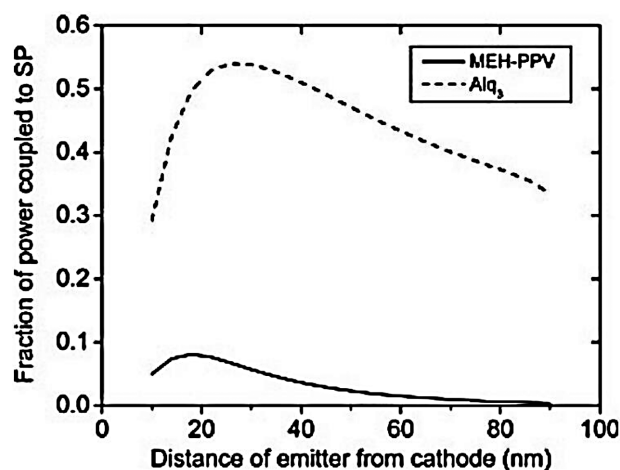


Figure 3 The calculated fraction of power lost from radiative excitations to surface plasmon modes is shown as a function of position of the excitation within the organic layer. Data are shown for the two generic OLED structures based on the small molecule Alq₃ and conjugated polymer MEH-PPV (with permission of Ref. [47]. Copyright 2002 WILEY-VCH Verlag GmbH & Co. KGaA, Weinheim).

small molecules depends on the shape of the molecules, such as the linear shape is preferred to the horizontal orientation. Therefore, it's not a universal strategy to improve the outcoupling.

Considering the 40% loss for most of the small molecule-based OLEDs, SPPs represent a potentially very serious limitation on the OLED performance. A metal-free OLED could be a solution for the purpose of reducing the SPP loss, for example, transparent OLEDs with transparent conducting oxide as both top and bottom electrodes [82–84]. However, higher cost and complex fabrication process of the tin oxide-based compounds limit their use in the OLEDs. Moreover, the metallic electrode with high reflectivity itself plays an important role in obtaining high efficiency of the OLEDs by redirecting the light emitted

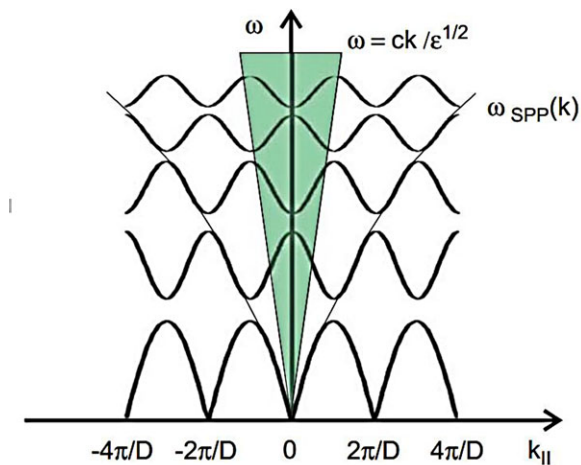


Figure 4 Schematic of the SPP dispersion on a periodically structured surface (period D) demonstrating SPP band-gap formation. SPP dispersion on a smooth surface is shown by the thin solid line (with permission of Ref. [74]. Copyright 2004 Elsevier B.V.).

from the opposite transparent electrode. On the other hand, ITO-free OLEDs by employing metallic film with high electrical conductivity and optical transmission as both top and bottom electrodes to replace tin oxide [85, 86] could not only realize a lower-cost fabrication process but also eliminate the power lost to the WG modes in high-refractive-index ITO film. In this case, light trapped in the SPP modes become the main power loss for this type of OLEDs. The SPP loss can be directly reduced by increasing the distance between the emitter and the metallic electrode by increasing the thickness of the emitting or transporting layers as shown in Fig. 3, which results in a reduced coupling between the emitter and the SPP mode due to the exponential decay of the SPP field in the dielectric medium. However, considering the low carrier mobility of the organic thin film, increased thickness of the emitting or transporting layers would result in a decreased internal quantum efficiency of the OLEDs.

2.3. Light extraction by the micro/nano patterns

Micro/nano patterns with both periodic and random structure could be used to increase light extraction of an OLED. An appropriate periodicity such that waveguided light is Bragg-scattered into the forward direction is required for the periodic micro/nano patterns by satisfying the Bragg scattering condition [9, 87]. The appropriate periodicity of the micro/nano pattern integrated on the metallic electrode is crucial for outcoupling the power lost to the associated SPP modes at the desired light-emitting wavelength (Fig. 4). SPP resonance at the periodically corrugated metal surface is tunable by adjusting the grating period as the following condition, when the energy and momentum of the incident light match to that of the SPP mode along the metal/organic interface [74].

$$k_{spp} = \left| k_{light} \sin \alpha \pm \frac{2\pi m}{\Lambda} \right| \quad (2)$$

Where, k_{spp} is the in-plane wavevector of the SPP, k_{light} is the wavevector of the emitted light, Λ is the period of the corrugation, α is the emission angle, and m is an integer. The appropriate period of the micro/nano patterns is required to extract the WG or SPP modes in normal emission, so that their resonance at the normal direction could be close to the emission peak wavelength of the emitter in the OLEDs. However, SPP and WG modes would be coupled out of the structure at different wavelengths because of their different dispersion relation. Therefore, it's crucial to tune both SPP and WG to be within the emission wavelength region by designing the parameters of the device structure.

Micro/nano patterns with random structure such as nanoporous alumina [35, 36], spontaneously formed nanofacet-structured MgO and buckles [34, 37, 88], and random nanostructure scattering layers [89, 90] have been employed in OLEDs to realize the enhanced light extraction. Unlike the periodic structure to outcouple the photons at a particular wavelength region by satisfying the Bragg condition, the random structure with directional randomness and broad distribution can enhance the light outcoupling without introducing spectra changes and directionality.

3. The fabrication of micro/nano patterns in OLEDs

A simple and low cost manufacturing technique is crucial for introducing the micro/nano patterns into the OLED structure. Various lithography-based technologies are effective in fabricating periodic corrugation. However, these approaches are applicable in inorganic LEDs due to the high chemical and physical stability of the inorganic semiconductors, while difficult to apply to OLEDs because organic materials are soluble generally in the solvents used in the lithography, and they experience electrical and/or optical deterioration when exposed to oxygen, water or high-energy electrons. The feasible approaches to introduce the micro/nano patterns into the OLEDs will be discussed in this section. The fabrication techniques for integrating the micro/nano patterns in the OLEDs are mostly applicable to OPVs owing to their similar materials and device fabrication processes.

3.1. The fabrication of the periodic micro/nano patterns in OLEDs

3.1.1. Holographic lithography for the micro/nano patterns

Usually, the micro/nano patterning has to start from the substrate to avoid the degradation of the OLEDs, so that pattern transmits through the organic layer to the opposite electrode. Holographic lithography (or interference

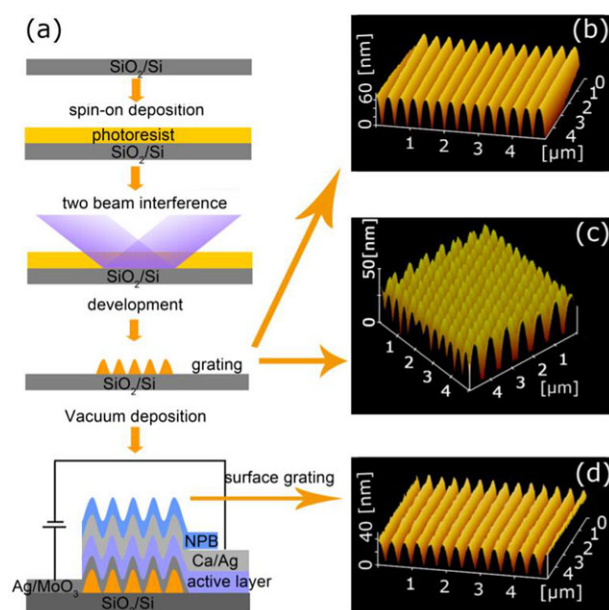


Figure 5 Scheme of introducing periodic corrugation into a TOLED by holographic lithography (a), and AFM images of the 1D (b) and 2D (c) grating on the photoresist surface and 1D grating on the Ag cathode surface (d) (with permission of Ref. [96]. Copyright 2012 WILEY-VCH Verlag GmbH & Co. KGaA, Weinheim).

lithography) is commonly used technique for fabricating the periodic micro/nano patterns. The photoresist-coated substrate was exposed by interference fringes. After development, the substrate was etched by RIE (reactive-ion etching) dry etching, and then the photoresist was removed. In case of the ITO coated substrate was used, the patterns can be directly introduced to the layer of the ITO anode by RIE etching [91]. Alternatively, The ITO or metallic anode was deposited onto the micro/nano patterned substrate and followed by organic and cathode layers to complete the device. Periodically corrugated OLEDs on silica substrates by holographic lithography followed with RIE dry etching have been reported [92–95]. Otherwise the periodic micro/nano patterned photoresist coated on the substrate can be directly used for the OLED deposition without the RIE dry etching (Fig. 5), which significantly simplified the fabricating process [46, 90, 96]. On the other hand, 2-D SiO₂/SiN_x photonic crystals have been fabricated by the holographic lithography and RIE etching (Fig. 6) [28–30]. The photonic crystals are inserted at the interface between the ITO layer and the glass substrate. In this case, the surface of the 2-D SiO₂/SiN_x photonic crystals is planar, and the pattern was not introduced to the following electrode and organic layers. Inserting a vacuum nanohole array into OLEDs by using a robust reverse-transfer process also maintained a planar profile of the functional layers [97].

The fabrication of the micro/nano patterns from the substrate is encountered with problems such as electronic degradation, because the surface roughness of the ITO anode sputtered on the corrugated substrate is increased. It is obvious that the problem may be solved if direct patterning

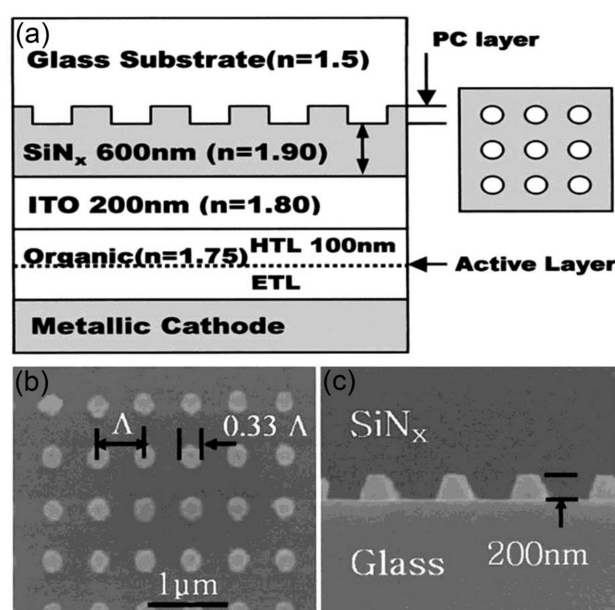


Figure 6 (a) The layer structure of a PC-OLED with SiN_x and SiO₂/SiN_x PC layers. Scanning electron micrographs: (b) top view and (c) cross-sectional view of the PC-OLED layers (with permission of Ref. [29]. Copyright 2003 American Institute of Physics).

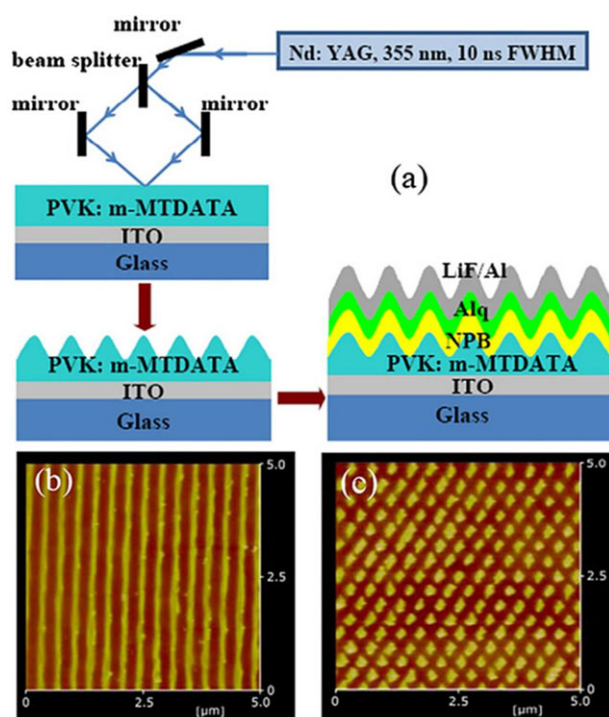


Figure 7 Scheme of introducing periodic corrugation into OLED by laser ablation (a), and AFM images of the ablated corrugation, 1-D (b) and 2-D (c) grating with period of 350 nm on the HTL surface (with permission of Ref. [101]. Copyright 2011 Elsevier B.V.).

of a certain organic functional layers of the OLEDs can be realized without affecting the flatness of the ITO film. Most polymers are strongly sensitivity to UV laser ablation condition with low ablation thresholds, so that a corrugation can be directly recorded on the functional layers of OLEDs via laser ablation. The one-step fabrication of the periodic corrugation can be faster and highly reproducible with the period from microns to sub 100 nm through combining with a multi-beam interference [98–100]. The periodic corrugation with appropriate depth and period for Bragg scattering in OLEDs are easily obtained by adjusting the laser fluence and the angle of the two laser beams, as shown in Fig. 7 [101]. The one-step laser ablation on organic functional layers provides a facile and simple approach with high controllability, high resolution and reproducibility to obtain periodically micro/nano patterned OLEDs. The one-step directly laser ablating of the hole-transporting layer of the OLEDs to introduce the micro/nano patterns has demonstrated three times efficiency enhancement [101].

3.1.2. Nanoimprint lithography in OLEDs

Nanoimprint lithography (NIL) as another one-step fabrication approach provides a simple way of micro/nano patterning the functional layers of the OLEDs. High-resolution patterning of both polymer light-emitting media and small molecule by using the thermal, vacuum or ultraviolet NIL has been reported [102–105]. Reboud et al. [105] reported that the patterned functional polymer layers can be reversely imprinted onto metallic electrode by using the thermal NIL techniques (Fig. 8). The Alq₃ (8-hydroxyquinoline aluminum) /DCMII gratings with a period of 200 and 300 nm by the nanoimprint exhibited no degradation in the luminescent efficiency [106]. The patterns were introduced to dendrimer-based OLEDs by the NIL [48]. Polymer distributed feedback lasers were demonstrated by using the NIL-fabricated wavelength-scale microstructures [107]. The close-packed array of polystyrene microsphere can be used as template for the PDMS replica [35]. While for the NIL-induced micro/nano patterns in the OLEDs, the effects of the temperature and pressure environment on the optical and electrical property of the organic materials should be considered.

3.1.3. Other methods

Several methods other than the above mentioned technique have been reported to introduce the periodic micro/nano patterns into the OLEDs. microlens array was usually made by using a mold transfer process, which is typically a combination of lithography, thermal reflow, molding and UV or thermal forming methods [12, 108–110]. Periodic change of the refractive index without surface-relief structure has been inscribed in the active materials in the OLEDs by holographic setup to modify the output characteristics of the OLEDs [111]. However, this method is limited by realizing a polymer with both charge-transporting and photosensitive

qualities to undergo a photoisomerization and act as functional layer in OLEDs. Colloidal lithography was employed to integrate a monolayer of SiO₂ microspheres on the substrate of the OLEDs to extract the substrate mode [15–17]. The functional films of the OLEDs can be direct patterned by the colloidal lithography. A close-packed monolayer array of polystyrene microsphere was etched into a non-closely packed monolayer array, and a thermal deposition of WO₃ [36, 112] on the PS monolayer results in a hexagonally perforated anode modification layer on the ITO anode. Using the monolayer colloidal crystal as template for the chemical etching of the ITO resulted in a large-area nano-structured ITO anode [113]. E-beam lithography-fabricated periodic arrays of Al nanorods [114] and circular metallic gratings [115] and focused ion beam milling-fabricated Ag gratings [116] have explored their applications in OLEDs or OPVs. Both methods have high resolution in generating nanoscale structures, while have the disadvantages of low throughput and high cost. Photolithography could be used for pixilation of the OLEDs with micro size for displays [117], while it's difficult to realize the patterns in sub-wavelength scale.

3.2. Fabrication of random micro/nano patterns in OLEDs

Several simple and low-cost processes without an additional lithography or patterning process have been reported to obtain the spontaneously formed random micro/nano patterns. MgO nanofacets as random micro/nano patterns (Fig. 9) can be formed spontaneously due to the anisotropic material characteristics of MgO between crystal orientations [38]. A thin film of MgO was inserted between the ITO layer and the glass substrate by electron-beam evaporation. The MgO facet was formed due to anisotropy of the properties between (111) and the other main planes of MgO, (200) and (220). The nanofacet-structured MgO film acted as a refractive-index-modulating layer to reduce the total internal reflection at the ITO/glass interface. Takezeo et al. [41, 45] reported spontaneously formed buckles as another kind of random micro/nano patterns introduced into the OLEDs. Buckling patterns are realized by thermally evaporating aluminium films on PDMS substrates, which is preheated to 100°C using an external radiation source. After cooling to ambient temperature, buckling spontaneously occurred. Using nanoporous anodic aluminium oxide [39, 40, 118], alumina nanohole array [119] or randomly distributed dewetting Ag droplets as a hard mask [42, 44] are alternative methods to introduce the random micro/nano patterns into the OLEDs.

From a practical point of view, high-resolution, simple, low-cost and high-throughput techniques to fabricate the micro/nano patterns are required for the commercialization and need to be pursued and developed. Holographic lithography [90–96] and nanoimprint lithography [102–107] deliver high quality, inexpensive and large area periodic micro/nano patterns, and could be easily applied to OLEDs. For random pattern fabrication, spontaneously formed

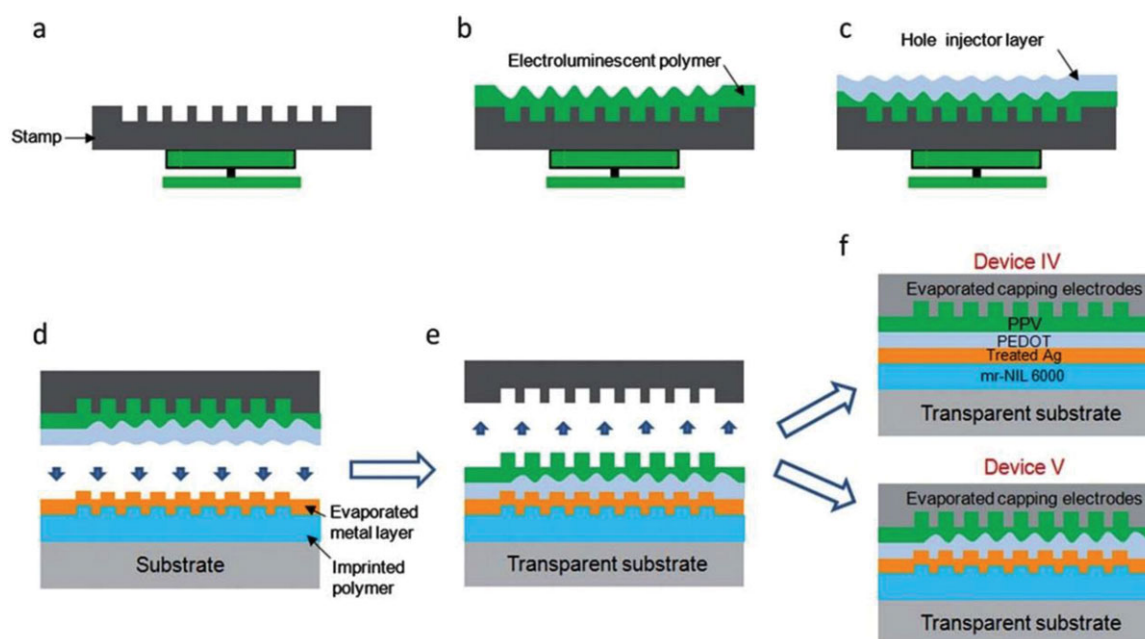


Figure 8 Schematic of process steps based on reverse nanoimprint for the fabrication of OLEDs. (a) The silicon stamp is placed on a spin-coater, (b) light-emitting polymer (PPV) is spin-coated on the stamp, (c) PEDOT is spin-coated on top of the PPV layer, (d) the spin-coated stamp is reverse imprinted on a unpatterned or patterned pre-treated metallic surface fabricated by conventional thermal NIL techniques, (e) the stamp is carefully separated leaving the polymer multi-layers on the metallic electrodes and (f) the cathode is evaporated to form the OLEDs. Devices IV and V incorporate an unpatterned and patterned anode (with permission of Ref. [105]. Copyright 2012 The Royal Society of Chemistry).

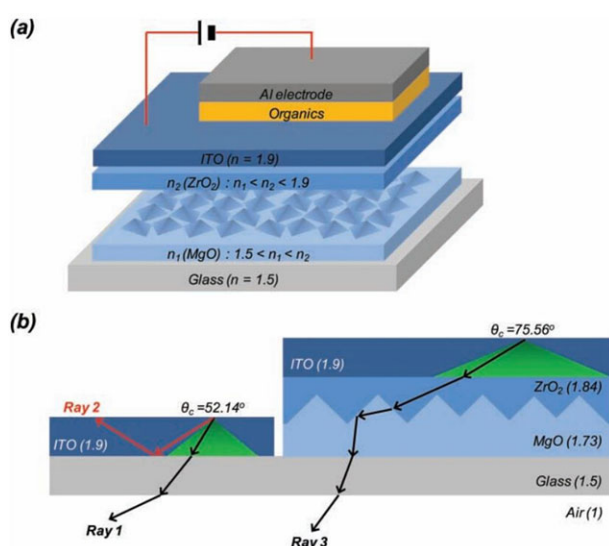


Figure 9 (a) Schematic diagram of bottom-emitting OLEDs with the embedded nanofacet-structured refractive index modulation layers (RIML) at the glass/ITO interface. The RIML is composed of electron-beam-evaporated MgO and MgO/ZrO₂. (b) Schematic explanation of the mechanism for improving device out-coupling efficiency with a microfacet-structured RIML. Diagrams are not to scale (with permission of Ref. [38]. Copyright 2010 WILEY-VCH Verlag GmbH & Co. KGaA, Weinheim).

random patterns [38, 41] and hard mask template [39, 40] provide inexpensive and simple methods for the potential industry applications.

4. Enhanced device performance by micro/nano patterns

4.1. External light extraction from OLEDs by the micro/nano patterns

To outcouple the photons trapped inside the substrate of the bottom-emitting OLEDs due to the total internal reflection at the glass/air interface, a modification of the external surface of the glass substrate are often preferable since they do not induce any alteration either in the functioning or in the architecture of the device. In particular, there is neither any change on device electrical properties nor spectral variation with viewing angle. The effect of the micro/nano patterns, with different feature size and geometries, in the light extraction has been discussed by different authors. Microlens arrays [120–125], micrometric conical pillars [126], micrometric and millimeter size pyramids [127, 128] have already been employed to this purpose. Among these geometries, microlens array is simple to fabricate and can be easily applied to large area substrates. Theoretical and experimental works have been developed to quantitatively analyze the performance of the microlens array with various shapes

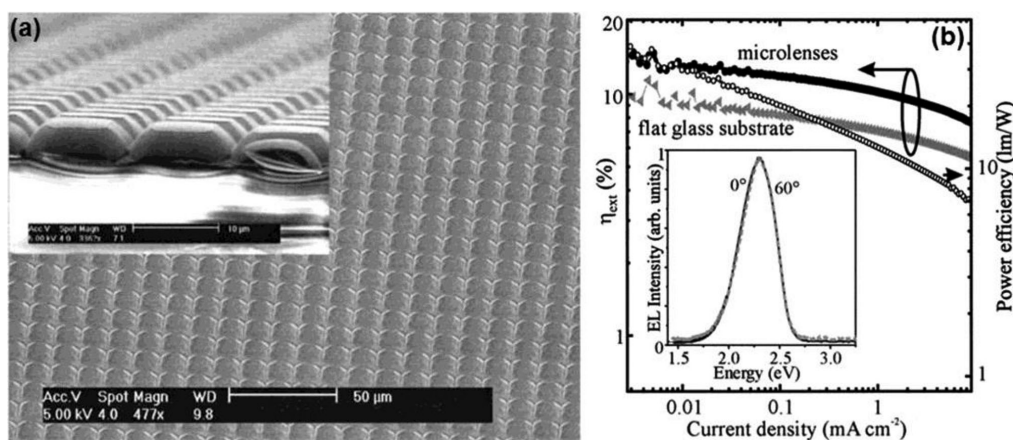


Figure 10 SEM of a PDMS microlens array fabricated from the mold. The detailed side view of the lenses (inset) shows that the PDMS accurately images the mold shape. External quantum and power efficiency vs current density of an Ir(ppy)₃ doped phosphorescent OLED (with permission of Ref. [13]. Copyright 2002 American Institute of Physics).

and sizes for the light extraction enhancement of planar OLEDs by comparing the efficiency of the devices with and without the microlens array. The enhancement of light extraction of up to 85% was theoretically predicted from an optimized lens pattern with a hemispherical structure [109]. Experimentally, Forrest et al. [13] demonstrated a 50% EQE enhancement with the EQE increasing from 9.5% to 14.5% by using a 10 μm diam PDMS lenses attached to the glass substrates of a *fac* tris(2-phenylpyridine)Iridium (Ir(ppy)₃)-based OLED (Fig. 10). Uniform 2 μm-pitch microlens arrays resulted in a 100% EQE enhancement [110].

In addition to the microlens array, incorporation of other micro/nano patterns to the back side of the substrate to outcouple the substrate mode was investigated. The submicrometer-size silica spheres with monolayer of hexagonally closed-packed arrays [15–17] attached to a glass substrate effectively scatter waveguided light within a glass substrate and resulted in a 60% enhancement in luminous efficiency for the Alq₃-based OLEDs [17], 22% enhancement in outcoupling efficiency by using a diffusive layer [129] and 40% enhancement in current efficiency by using pillar arrays [130] have been observed, respectively. Shaping of the device into a mesa structure demonstrated 90% improvement in the EQE [64]. It should be pointed out that the incorporation of the micro/nano pattern to the back side of the substrate induces blurring of the image due to the light rays are outcoupled from the non-emissive region. This may not be desirable for high resolution displays.

4.2. Internal light extraction from bottom-emitting OLEDs

The modification of the internal structure inside the device is required to achieve the internal extraction of the power loss to the light waveguiding in the ITO/organic layer or the SPP mode at the organic/electrode interface. The effect of the internal structure modification by the micro/nano pat-

terns on the internal light extraction of the bottom-emitting OLEDs will be discussed in this section.

4.2.1. Outcoupling of the WG and SPP mode in OLEDs

If the micro/nano patterning starts from the substrate, the following deposited organic layers and electrode by thermal evaporation duplicate morphology of the substrate. The transmission of the corrugation through the organic layers to the opposite electrode is crucial for the simultaneous outcoupling of the WG and SPP mode. Additional peaks corresponding to the SPP or WG resonance can be observed from the EL spectra of the OLEDs, which indicate an efficiently outcoupling of photons from these optical modes [90, 92, 101, 131]. For emission normal to the OLED structure, an additional peak corresponding to the SPP or WG resonance at the normal direction can be observed within the emission wavelength region of the OLEDs, and at other angles the peak splits into two features—one at shorter wavelength and the other at longer wavelength for both SPP and WG modes, as can be seen in Fig. 11 [101]. These optical modes can be identified by the simulated spatial magnetic field distribution across the device structure as a function of position with the normal incident light [46, 96, 101]. The field intensity corresponding to the SPP resonance is with maximum at the metallic electrode/organic interface and decay along the direction perpendicular to it (Fig. 2). On the other hand, the field confined mainly within the organic and ITO layers should be assigned to the TE and TM polarized WG modes due to the high refractive index of the organic and ITO layers. It should be noted that the angular-dependent resonant wavelength of both WG and SPP modes would result in an angular dependence of the EL spectra, which may cause an angular-dependent color change as this would be undesirable for display applications. While, only the resonant wavelength within the emission wavelength region of the emitter can be coupled out for both SPP and WG mode, which weaken the influence

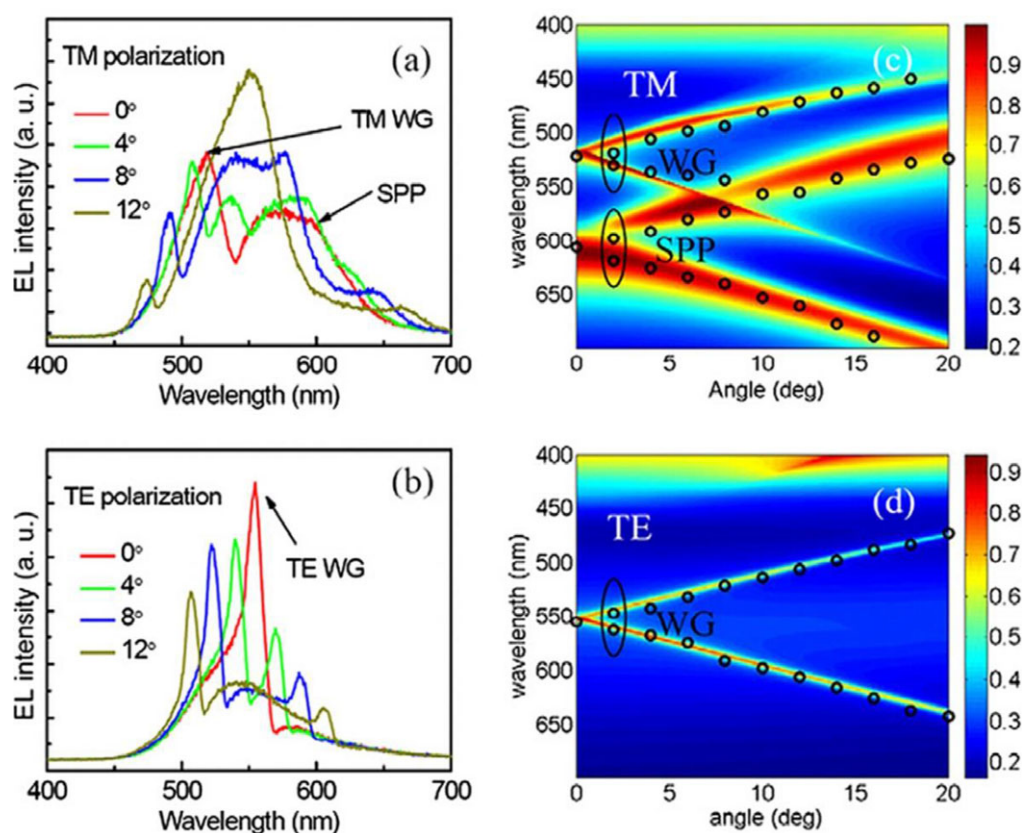


Figure 11 Measured EL spectra with TM (a) and TE (b) polarization at different observation angle from the corrugated OLEDs with 350-nm grating. And the wavelength versus incident angle for the calculated dispersion relation of the corrugated OLEDs for TM (c) and TE (d) polarization. The measured dispersion relation extracted from the EL spectra (circles) is also shown in (c) and (d) (with permission of Ref. [101]. Copyright 2011 Elsevier B.V.).

of the angular-dependent EL on the color change. On the other hand, a well-designed micro/nano pattern would scatter the modes across the whole spectrum to improve the viewing characteristics, which is discussed in Section 4.2.2 and 4.3.

In case of a periodic micro/nano pattern is introduced, besides the grating period, the amplitude of the grating is an important factor to affect the light extraction efficiency of the OLEDs [88, 89, 132]. The optimal depth for the optical and electrical properties is usually not coincident. It would seem likely that the increased grating depth would lead to a larger thickness variation for the following deposited organic functional layers and electrode. The resulted non-uniform electric field distribution leads to a non-uniform current flow across the organic layers and a degradation of the OLED performance. Considering the thickness of the organic films of a typical OLED is around 100 nm in total, the optimized grating depth is in the region of a few tens nanometers [37, 46, 133]. Efficient outcoupling of the SPP and WG modes has been demonstrated for the micro-nano patterned OLEDs based on polymer [46], small molecules [92, 101] and phosphorescent dendrimers [48]. Worthing and Barnes [134] reported that only approximately half of all propagation directions can couple to radiation for SPPs

propagating on a 1-D corrugated surface, which limits the SPP radiation efficiency. Whereas in case of 2-D corrugation, SPPs propagate all in-plane directions can be coupled to free-space radiation, resulting in improved coupling efficiency. Higher EL intensity from the 2D-patterned OLED compared to that of the 1D-patterned OLEDs was observed [92]. The outcoupling of the WG modes is also more efficient for the 2D patterns. Youn et al [135] reported a scheme to extract both the WG and SPP modes simultaneously by fabricating OLEDs on corrugated high-refractive-index sapphire substrates, and a high EQE of 63% was obtained by using an additional macro lens on the back side of the substrate.

Unlike the periodic corrugation formed throughout the OLED structure, the surface of the 2-D SiO₂/SiN_x photonic crystals inserted at the interface of the glass and the ITO anode was flattened by deposition of the SiN_x film using plasma-enhanced chemical vapor deposition (PECVD) [28] or a spin coating of a planarization layer [32]. The pattern was not introduced to the following electrode and organic layers, which is benefit to the electrical properties of the OLEDs. By comparing the OLEDs on both conventional substrate and a photonic crystal layer covered substrate side by side, an increase in the extraction of over 50%

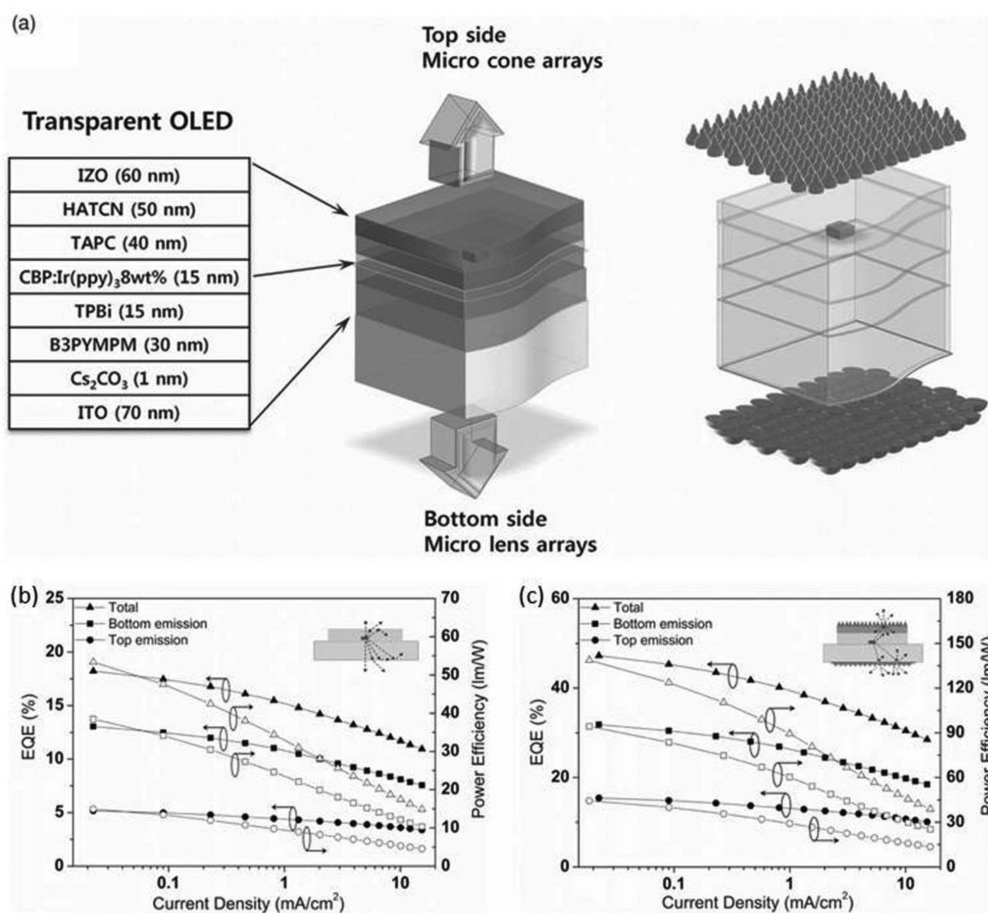


Figure 12 (a) Schematic diagrams of the structure of the transparent OLED and the microstructures for light extraction. (b-c) External quantum efficiencies and power efficiencies of the OLEDs (with permission of Ref. [12]. Copyright 2013 WILEY-VCH Verlag GmbH & Co. KGaA, Weinheim).

was achieved experimentally, and over 80% is expected theoretically [28, 29, 31–33]. For example, the current efficiency in the normal direction at 20 mA/cm² was improved from 10.9 cd/A for the conventional OLED to 16.4 cd/A for the 2D PC OLED corresponding to a 52% enhancement [31]. The improved outcoupling originates from the liberation of the photons trapped in the high-index ITO/organic WG mode. Meanwhile, with appropriate parameters of the PC structure, light waves tend to diffract more into shallow angles, which results in the light extraction from the substrate mode by reducing the total internal reflection, so that a high outcoupling efficiency is achievable. While the corrugation was not introduced to the electrode/organic interface, the SPP mode cannot be effectively outcoupled.

In case of the ITO-free OLEDs with two metallic electrodes, a metallic film with high electrical conductivity and optical transmission is used to replace ITO as anode. Highly efficient light extraction could be expected by excitation and outcoupling of the SPP modes in the OLEDs, since light trapped in the SPP modes becomes one of the main power lost [90, 131, 136]. A 30% current efficiency

enhancement was obtained by increasing the efficiency from 3.2 to 4.19 cd/A for the Alq₃-based OLEDs with two metallic electrodes of Au anode and Ag cathode, where the SPP losses at the Ag cathode/organic interface were effectively extracted by introducing the periodic micro/nano patterns [137]. On the other hand, a metal-free OLED with good transparency combined with a method to extract the light efficiently from the device could be another solution for the purpose of reducing the SPP loss [138]. Kim et al. [12] reported the transparent OLEDs with the indium zinc oxide (IZO) and ITO layers as the top and bottom electrodes, respectively. A high refractive index light extraction pattern was additionally fabricated on the transparent top electrode using a simple evaporation method and a microlens array sheet was attached on the bottom side of the glass substrate to extract the confined light inside the device, as shown in Fig. 12a. The resulted EQE of the OLEDs was increased from 18.2% to 47.3%. It was further improved to 62.9% by attaching an index-matched hemisphere lens instead of the microlens array on the glass substrate to extract the remaining light guiding losses inside of the device (Fig. 12b and c).

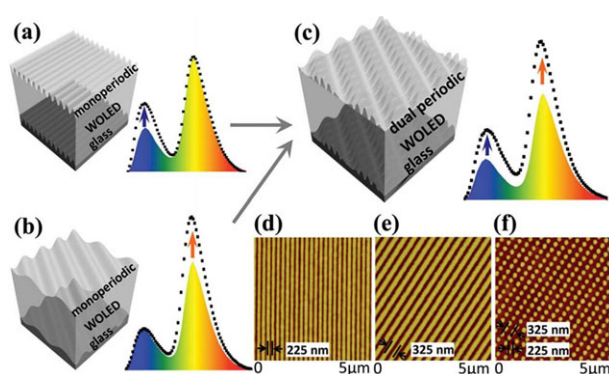


Figure 13 (a–c) Schematic of the broadband light extraction by using dual-periodic corrugation. (d–f) AFM images of surface morphologies of photoresist with 1D period of (d) 225 and (e) 325 nm, and (f) 2D dual-periodic corrugation (with permission of Ref. [139]. Copyright 2013 WILEY-VCH Verlag GmbH & Co. KGaA, Weinheim).

4.2.2. Broadband internal light extraction from OLEDs by micro-nano patterns

Broadband light extraction is important for the efficient outcoupling of the photons trapped in the white organic light-emitting devices (WOLEDs) with spectra covering the whole visible wavelength. Broadband extraction of the substrate modes can be easily realized by attaching a microlens array on the outside of the substrate. While broadband extraction is difficult to be obtained for the WG and SPP modes inside of the OLEDs by introducing the structure modification inside the device structure. Micro/nano patterns with monoperiodicity introduced into the OLEDs are suitable for specific narrow range of wavelength by satisfying the Bragg scattering condition, and applicable only for monochromatic OLEDs.

Broadband excitation and outcoupling of the SPPs in the WOLEDs have been obtained by introducing a 2-D pattern with dual-periodic corrugation into the WOLEDs [139]. The 2-D pattern consisted two sets of corrugations with different periods can broaden the SPP resonance compared to that of the monoperiodic pattern (Fig. 13). The blue and orange emission are both efficiently extracted from the two complementary color-based WOLEDs by tuning appropriate periods of the dual-periodic patterns. The maximum current efficiency was improved from 16.27 cd/A for the conventional planar devices to 22.33 cd/A for the dual-periodic corrugated device corresponding to 37% enhancement. Broadband Lambertian emitters have been obtained by using defective hexagonal-closed-packed grating for light extraction due to the periodicity broadening and the random orientation in the gratings, which resulted in enhancements in current efficiencies by a factor of 1.7 (from 2.57 to 4.38 cd/A) [35]. Random micro/nano pattern [140–142], such as nanoporous [39] or spontaneously formed quasi-periodic buckling [41, 143, 144], metal oxide nanostructures [145] or nanofacet structures

[38] have a broad distribution to enhance the light extraction efficiency without introducing spectral changes and directionality. Koo et al. [41] reported an EL spectrum enhanced by at least a factor of two across the entire visible wavelength regime by using the quasi-periodic buckles (Fig. 14). In the Alq₃-based devices with and without buckling, the current efficiency was 1.67 and 3.65 cd/A, respectively, corresponding to an enhancement of 120%. Metal nanoparticles induced localized surface plasmon resonance also support the broadband SPP excitation and can be embedded into the OLEDs [146–153]. Implementing quasi-periodic subwavelength nanofunnel arrays on the hole-injection layer of PEDOT:PSS via soft nanoimprinting lithography enhance broadband light extraction in WOLEDs [154, 155]. Inserting a nanosized strip auxiliary electrode layer between the substrate and ITO layer [156] or a plasmonic cavity having deep subwavelength nanostructures [157] is also able to enhance light extraction of WOLEDs.

In case of flexible OLEDs, broadband light extraction has been obtained by using an ameliorated low-refractive-index PET substrate consisting of a built-in transparent conductive electrode of Ag network and a bioinspired optical coupling layer of moth-eye nanostructure [158]. A composite electrode to replace ITO comprising a layer of single-walled carbon nanotube and a layer of silver nanowires embedded in the surface of a barium strontium titanate nanoparticle-polymer composite is also effective in flexible polymer-based OLEDs to realize broadband light extraction [159].

4.3. Light extraction from top-emitting OLEDs

Another way of outcoupling the trapped light is the use of microcavity structure to direct light emission to air. For the bottom-emitting OLEDs, aperiodic dielectric stacks were placed between transparent anode and glass substrate to increase the outcoupling efficiency by confining the emission within the narrowed viewing cone [160, 161]. In case of top-emitting organic light-emitting devices (TOLEDs), the top semi-transparent metallic electrode and the bottom metallic electrode together with the organic layers form a Fabry-Perot resonator, and the resulting microcavity resonance has a positive effect on the light outcoupling efficiency in the resonance region [162, 163]. However the microcavity structures usually resulted in non-Lambertian emission characteristics with obvious spectra shifts as a function of the viewing angle. TOLEDs are attracting much attention since light outcoupling from the top allows the fabrication of OLEDs on opaque substrates. It is particularly suitable for active matrix displays with high resolution and high information content due to the higher aperture ratio and display image quality. The simultaneous achievement of enhanced efficiency, enhanced color saturation and stable spectra with the viewing angles in the same device design is one of the main challenges for the practical applications of the TOLEDs [164–168].

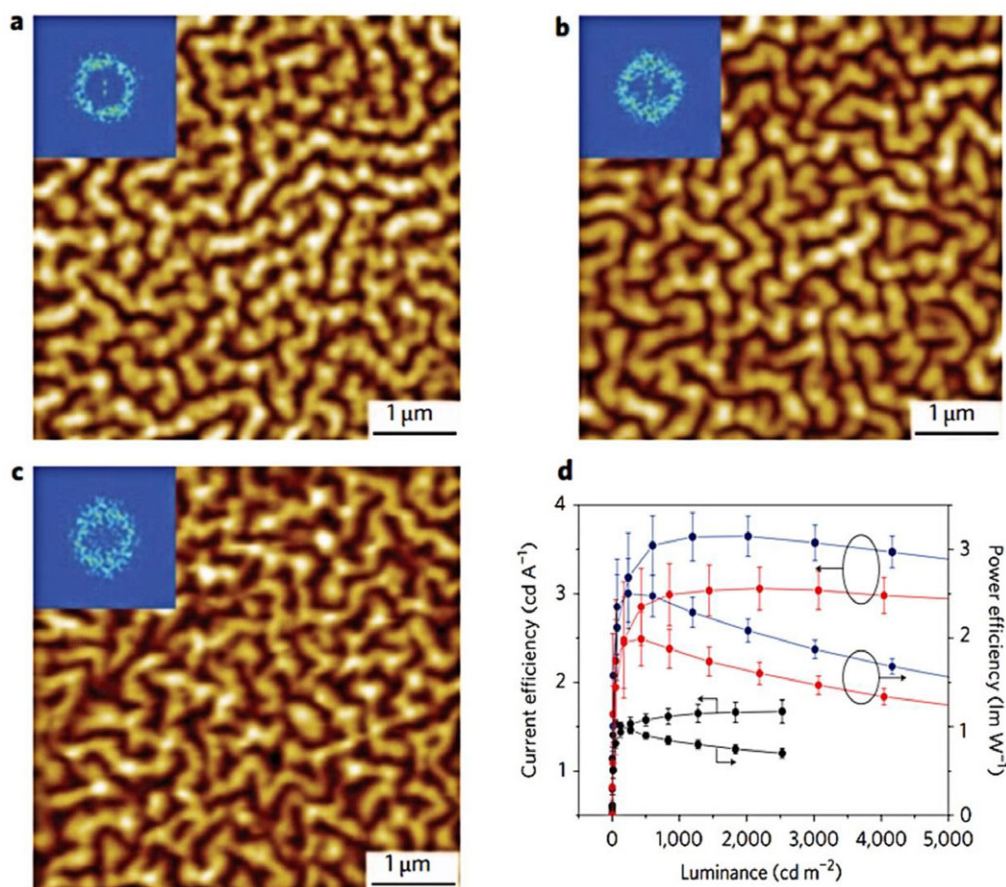


Figure 14 (a–c) AFM analysis of buckling patterns. Inset: FFT patterns of each image. (d) Current efficiency and power efficiency as a function of luminance for OLEDs without buckling (black) and with double (red) and triple (blue) buckling (with permission of Ref. [41]). Copyright 2010 Nature Publishing Group).

The metallic film is used as semi-transparent top cathode of the TOLEDs, and thinner metallic film ensures a higher transparency. However, more pinholes are formed in the very thin film due to its poor film continuity, which results in decreased electrical conductivity and lowered device efficiency. Thicker metallic film offers higher film continuity and thereafter higher electrical conductivity, however, the efficiency is still lowered due to the decreased optical transmittance. Jin et al. [96] reported an enhanced light transmission through a thick metallic cathode by cross coupling occurring between the SPP modes associated with the top surface of the cathode and the microcavity modes within the device induced by the periodic micro/nano patterns. An emitting layer of (4-(dicyanomethylene)-2-t-butyl-6-(1, 1, 7, 7-tetramethyljulolidyl)-4H-pyran (DCJTb) doped Alq₃ was employed for the red-emitting TOLEDs. As a result, the current efficiency at the current density of 100 mA/cm² is increased from 5.3 cd/A for the planar device to 7.1 and 7.4 cd/A for the 1-D and 2-D corrugated devices, respectively, which corresponded to 30% and 40% efficiency enhancement to the planar device by using the 1-D and 2-D corrugation. The half-luminance lifetime was

also much enhanced due to the increase of the cathode thickness.

Enhanced outcoupling efficiency of the TOLED has also been demonstrated by integrating a refractive index-matched microlens array on the top cathode [169, 170]. The microlens film with a higher index of refraction allows a large portion of the WG modes in the organic/transparent electrode layers to enter the microlens and be subsequently extracted. As we have discussed in Section 4.1, the microlens array on the glass substrate of the bottom-emitting OLEDs results in serious image blurring. In contrast, the blurring of pixel emission is substantially reduced for the case of TOLEDs laminated with microlens array. Realizing white emissions from TOLEDs has been encountered with challenges in not only the light extraction but also the high quality of the white color. The microcavity (MC) effect of the TOLEDs induces a narrow bandwidth of the EL spectrum as well as a blue shift of the emission color as the viewing angle increases. Broadband light extraction and stable colors with viewing angles have been obtained by using the microlens array in the TOLEDs. Therefore, this method is applicable to the white TOLEDs [124]. Another simple and

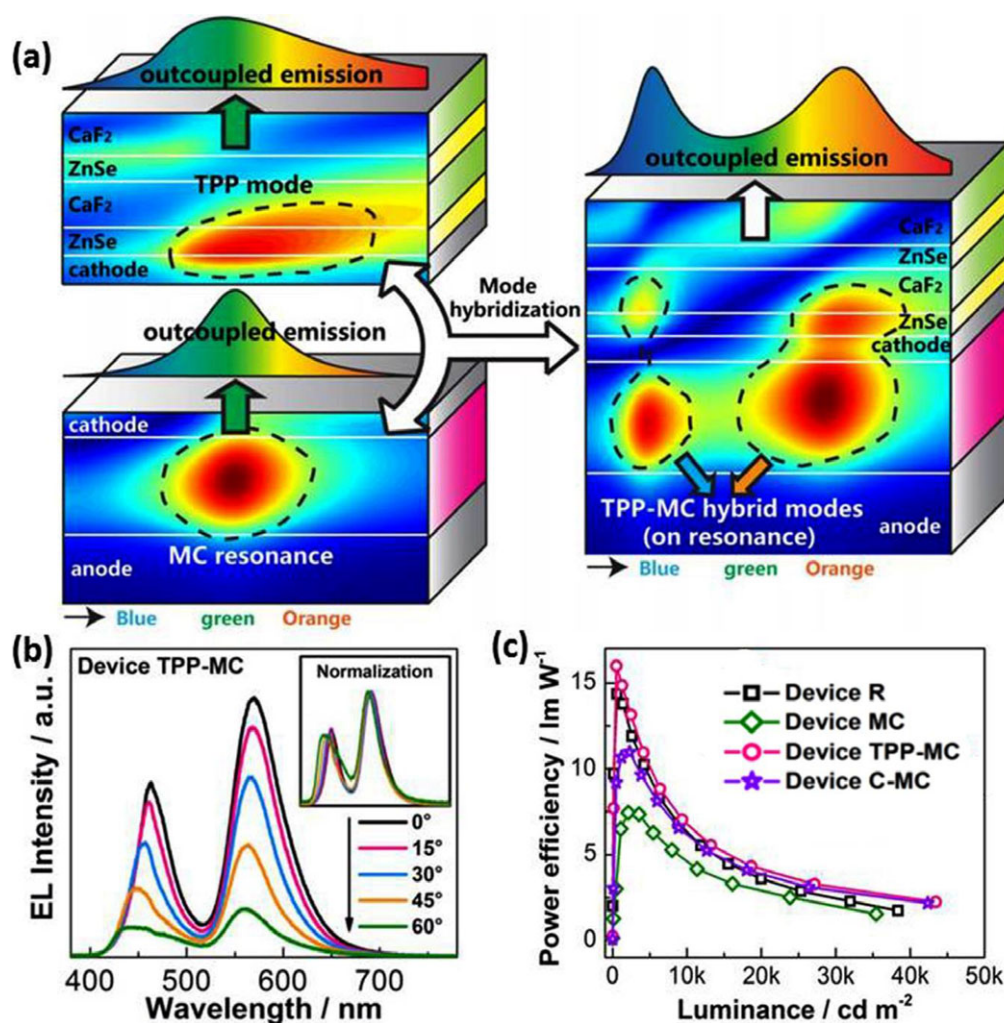


Figure 15 (a) Schematic of the mode hybridization strategy for the WOLEDs. (b) EL spectra of the device TPP-MC with various viewing angles. The normalized spectra are shown in the inset. (c) luminance–power efficiency characteristics of the bottom-emitting WOLED with ITO as the anode (device R), conventional MC-based device (device MC), WOLED based on the TPP-MC hybrid modes (device TPP-MC), and MC device with a capping layer (device C-MC). (with permission of Ref. [171]. Copyright 2015 Optical Society of America).

effective strategy [171] for WOLEDs with the improvement in both viewing characteristics and light outcouplings is based on a mode hybridization induced hybrid Tamm plasmon-polariton/microcavity (TPP-MC) modes (Fig. 15). The TPP-MC hybrid modes can be excited through the mode hybridization between the intrinsic MC resonance and the introduced TPP mode by integrating a photonic crystal structure upon the top metallic electrode to introduce the TPP mode as shown in Fig. 15a. The two excited TPP-MC hybrid modes are especially suitable for use in the WOLEDs based on two-complementary-color strategy, since they exhibit comparable light outcoupling efficiency while the resonant wavelengths could be simply designed to well match the intrinsic emission peaks of the WOLEDs. The two emission peaks on the EL spectra of the device both exhibit a slight blue shift as the viewing angle increases, but their intensity ratio is almost invariant

as can be seen in Fig. 15b. This feature results in a small variation of the CIE coordinate. The WOLEDs based on the hybrid modes exhibits the highest efficiency as a result of efficient light outcouplings (Fig. 15c).

In addition, introducing the micro/nano patterns into the TOLEDs provide another strategy to improve the viewing-angle characteristic by constructing a microcavity with a gradually changed cavity length [172, 173]. The microstructured cavity with gradually changed resonant wavelengths covering the whole visible range was constructed by two periodically corrugated Ag electrodes with different groove depth and sandwiched with organic layers. In this case, the period should be larger than wavelength scale to avoid disturbing the flat and wide band emission by Bragg scattering in the visible region. Both monochromatic and white TOLEDs with omnidirectional emission have been successfully obtained. A random nano-structured scattering layer

in TOLEDs is also effective in improving the out-coupling efficiency and spectra angular independency [174]. Compared to the micro/nano patterns, introducing a capping layer on top of the thin metallic cathode [164,165] is another effective method to improve the outcoupling efficiency and viewing characteristics by broadening the MC resonance. A broadened EL spectrum and increased outcoupling efficiency could be obtained by using the capping layer. An appropriate thickness and refractive index for the capping layer is required for the light outcoupling at specific wavelength or broadband light extraction.

The reported enhancement in the outcoupling efficiency of the OLEDs integrated with various mic/nano patterns has been summarized in Table 1. There exist variations in the materials, structure design and the fabrication process of the micro/nano-patterned OLEDs, and these factors should be taken into account for evaluating the various patterns on the light extraction. Despite the benefits of the micro/nano pattern-enabled light extraction discussed in the above sections, it should be noted that the performance reported for many micro/nano pattern-integrated OLEDs is still lower than the experimentally achieved efficiency records for OLEDs employing the same materials, as the largest enhancement factors were observed when comparing with relatively poor reference devices. A combination of the external and internal light extraction method would result in a maximum outcoupling efficiency of the OLEDs [12, 145].

4.4. Manipulation of the emitting properties by the micro/nano patterns

Besides the manipulation of the micro/nano patterns on the light extraction and emission spectra, the manipulation on the polarization, energy transfer [175–177], and highly directional light beam [178–182] can be obtained in the OLEDs. Highly directional EL have been achieved in the TOLEDs by using a 2D periodically patterned silver film as a cathode and an organic dye with a narrow bandwidth of emission spectrum as an emitter [93]. The TOLEDs exhibited beam divergence of less than 4° and the beam direction is controllable by tuning the periodicity of the corrugation. The resonant excitation of the SPPs associated at the silver film interfaces contributes to the light transmission through the silver cathode and to the directional emission.

Andrew et al. [183] reported that energy transfer from donor to acceptor molecules can be enhanced by the mediation of the SPPs through the coupling of the SPPs on the opposite interfaces of a metal film. For the SPP-mediated energy transfer, acceptor and donor molecules can be located at opposite sides of a metallic film, which allows radiative energy transfer over distances of more than 100 nm. This energy transfer process is quite different from the Förster or Dexter nonradiative energy transfer, where the distance between donor and acceptor molecules should be less than 10 nm. The SPP-mediated radiative energy transfer has been employed in the TOLEDs [95]. The EL intensity

from the patterned TOLEDs shows 10 times enhancement compared to that of the flat TOLEDs, because the coupled SPPs on the opposite interfaces of the micro/nano patterned silver cathode act as an efficient energy transfer mediator from the donor to the acceptor. This energy transfer mechanism has been applied into organic photovoltaics with an external antenna layer to realize broadband enhanced absorption by mediating the energy transfer from the antenna layer to the active layer [184].

5. Micro/nano patterns in organic photovoltaics

Micro/nano patterns are widely used in OPVs, while they play a different role in manipulating light in OPVs compared to that of the light extraction in the OLEDs, i.e. light trapping. The active layer in the OPVs is inherently very thin due to the low charge-carrier mobility and small exciton diffusion length of most small molecular and polymeric materials [185, 186]. The thickness of the active layer is in turn limited, which lead to poor solar light absorption and low power conversion efficiency (PCE). Localized SPs excited in metal nanoparticles [187–189] or SPPs propagating at the metal/organic interface can concentrate and fold light into the thin absorber layer and increase the absorption by proper engineering the micro/nano patterns [190–194]. It yields new options for solar-cell design by permitting a considerable reduction in the physical thickness of solar photovoltaic absorber layers. The micro/nano patterns employed in the OLEDs are mostly applicable to the OPVs in not only the fabrication techniques but the effect of the light manipulation. Unlike the SPP-enabled absorption enhancement by the metallic NPs or gratings, dielectric NPs have been employed in the OPVs to improve the light harvesting. High refractive index TiO_2 NPs are commonly used to form the light-scattering film by inserting it between the electrode and active layer [195, 196], or embedded it in PEDOT:PSS as light-trapping electrode [197]. Compared to the dielectric NPs-based light scattering, plasmonic nanostructures have been more extensively investigated, because SPPs are strongly confined at the metal/organic interface and results in an efficient incoupling of light into the absorbers [198, 199].

Tuning the SPP resonance to the absorption region of the absorber layer is crucial for the most absorption enhancement for efficiently utilizing the SPP-enhanced light trapping. In contrast to metallic nanoparticles, periodically micro/nano patterned metal film forms a particularly interesting class, since their periodicity can be tuned to easily adjust the SPP resonance so that a coincidence between the SPP resonance and the absorption wavelength region of the absorber layer can be obtained to realize a maximum absorption enhancement. Therefore, using the periodically micro/nano patterned metal to excite SPP may provide a possible way to release the tradeoff between photon absorption and exciton harvesting efficiency. 1-D or 2-D periodic micro/nano patterned metallic electrode with wave

Table 1 Reported enhancement in the outcoupling efficiency of the OLEDs integrated with various micr/nano patterns

Micro/nano patterns	Efficiency enhancement	Ref. No.
Microlens array on back side of the substrate	50% (in EQE)	[13]
	100% (in EQE)	[110]
Microlens array on top electrode of TOLEDs	120% (in EQE)	[170]
	51% (in EQE)	[124]
Silica sphere on back side of the substrate	60% (in cd/A)	[7]
Pillar array on back side of the substrate	40% (in cd/A)	[130]
Mesa shaping of the device	90% (in EQE)	[64]
Periodic gratings inside the device structure	30% (in cd/A)	[137]
	37% (in cd/A)	[139]
	70% (in cd/A)	[35]
	40% (in cd/A)	[96]
2-D photonic crystals at the interface of the glass and the ITO anode	38% (in cd/A)	[28]
	52% (in cd/A)	[31]
Random patterns inside the device structure	120% (in cd/A)	[41]
	34.7% (in lm/W)	[38]
	40% (in EQE)	[140]
	70% (in EQE)	[145]
Top microcones array combined with bottom microlens array	160% (in EQE)	[12]
Random buckling inside the device structure combined with a hemispherical lens on back side of the substrate	150% (in EQE)	[145]

length-scale periodicity has been integrated into the OPV structure to excite the SPP at the metal/organic interface with tunable resonance. Yu Jin et al. demonstrated 35% enhancement in the PCE by employing a 1-D periodic micro/nano patterns [190, 191]. Various fabrication approach has been employed to introduce the 1-D and 2-D patterns into the OPVs, where the various grating conditions, such as dimensions, period and depth on the OPV performance was investigated [200–206].

Broadband excitation of the SPPs supported by the micro/nano patterns is highly desirable for the broadband absorption enhancement to improve the PCE of the OPVs. Dual plasmonic nanostructures with combined metallic NPs and metallic grating electrode [207, 208], and combined metallic grating and photonic crystal [209] have been reported to realize multiple SPP excitation. The micro/nano patterns with 2D dual periodic [210], aperiodic [211] and quasi-periodic corrugations [206], and hexagonal pyramid arrays [212] capable of light trapping with broadband spectra response by the effect of anti-reflection, light scattering as well as SPPs. 3-D ITO nanohelix array fabricated by an oblique-angle deposition technique has been applied in the OPVs as a multifunctional electrode for simultaneously improving light absorption and charge transport [213]. Using an external antenna layer with complementary absorption property to the active layer is another exam-

ple of the SPP-resulted broadband absorption enhancement [184]. The antenna layer absorbs the photons at shorter wavelength, which is coupled to the active layer by SPP mediated energy transfer through the micro/nano patterned metallic electrode. As a result, the absorption was enhanced in a wide wavelength range from 400 nm to 700 nm.

6. Conclusions and outlook

In this review, we have discussed the major advances that have recently been achieved in the light manipulation in OLEDs by integrating micro/nano patterns. By incorporating the micro/nano patterns with random or periodic morphologies inside and outside the device structure, the OLEDs show enhanced light extraction performance compared to the conventional planar devices for both bottom and top-emitting OLEDs. The photons trapped in the substrate of the bottom-emitting OLEDs due to the total internal reflection at the glass/air interface can be effectively outcoupled by a micro/nano patterned external surface of the glass substrate, while the power lost to the WG and SPP modes can be effectively outcoupled by the modification of the internal structure inside the device with the micro/nano patterns. Broadband light extraction in OLEDs and light

absorption in OPVs both can be obtained by micro/nano pattern-induced broadband excitation of the SPPs. In case of the TOLEDs, the micro/nano patterns play an important role in not only light extraction but improving the viewing-angle characteristic. We have further discussed emitting properties other than the light extraction could be manipulated by introducing the micro/nano patterns.

Due to the progress made in material development and device optimization, OLEDs have demonstrated remarkable success in the past few years with the recent advance in display industry. In the long term, research is moving from developing the materials to optimizing the light out-coupling from the design of the device structure. For further progress, the focus on the science and technology of micro/nano patterns for light manipulation offers the potential of achieving higher-efficiency devices, which is particularly important for lighting applications where high efficiency is critically required. We should also keep in mind that a simple and low cost manufacturing technique of the micro/nano patterned OLEDs is crucial for commercial applications. The authors hope that the subject of this review, summarizing the knowledge of light manipulation by the micro/nano pattern in the OLEDs, would be instrumental in optimizing structure design and, consequently, high-efficiency devices.

Acknowledgements. This work was supported by the National Nature Science Foundation of China (NSFC) and National Basic Research Program of China (973 Program) under Grants #61675085, #2013CBA01700, #61505065, and #61595930.

Received: 30 June 2016, **Revised:** 25 June 2016,
Accepted: 2 February 2017

Published online: 27 February 2017

Key words: Organic light-emitting devices, light extraction, micro/nano pattern, organic photovoltaics, light trapping.



Jing Feng received the B.S. and Ph.D. degrees in microelectronics and solid-state electronics from Jilin University, Changchun, China, in 1997 and 2003, respectively. From 2003 to 2006, she was a Postdoctoral Researcher with RIKEN, Japan. In 2006, she joined Jilin University, where she is currently a professor at the College of Electronic Science and Engineering and State Key

Laboratory on Integrated Optoelectronics. Her research interests have been focused on organic optoelectronic devices.



Yue-Feng Liu received the B.S. degree in electronics science and technology and the Ph.D. degree in microelectronics and solidstate electronics from the College of Electronic Science and Engineering, Jilin University, Changchun, China, in 2008 and 2014, respectively. In 2014, he joined Jilin University, where he is currently an assistant professor at the College of Electronic Science and

Engineering and State Key Laboratory on Integrated Optoelectronics. He has published more than 20 scientific papers in academic journals. His research interest includes organic optoelectronic devices.



Yan-Gang Bi received his B.S. degree in microelectronics (2010) from Jilin University. Now, he is a Ph.D. student in College of Electronic Science and Engineering, Jilin University. His current research is focused on the fabrication of microstructures via holographic lithography technique and the applications of microstructures in organic light-emitting devices and organic solar cells.



Hong-Bo Sun received the B.S. and Ph.D. degrees in electronics from Jilin University, China, in 1992 and 1996, respectively. He worked as a postdoctoral researcher in Satellite Venture Business Laboratory, the University of Tokushima, Japan, from 1996 to 2000, and then as an assistant professor in Department of Applied Physics, Osaka University, Osaka, Japan. In 2005, he was promoted as a full professor (Changjiang Scholar) in Jilin University, China. His research interests have been focused on ultrafast optoelectronics, particularly on laser nanofabrication and ultrafast spectroscopy.

References

- [1] C. W. Tang and S. A. VanSlyke, *Appl. Phys. Lett.* **51**, 913–915 (1987).
- [2] F. So and D. Kondakov, *Adv. Mater.* **22**, 3762–3777 (2010).
- [3] V. Coropceanu, J. Cornil, D. A. S. da Filho, Y. Olivier, R. Silbey, and J.-L. Brédas, *Chem. Rev.* **107**, 926–952 (2007).
- [4] C. Rothe, *Laser & Photon. Rev.* **1**, 303–306 (2007).
- [5] S. D. Yambem, M. Ullah, K. Tandy, P. L. Burn, and E. B. Namdas, *Laser Photon. Rev.* **8**, 165–171 (2014).
- [6] F. L. M. Sam, C. A. Mills, L. J. Rozanski, and S. R. P. Silva, *Laser Photon. Rev.* **8**, 172–179 (2014).
- [7] G. Xie, M. Chen, M. Mazilu, S. Zhang, A. K. Bansal, K. Dholakia, and I. D. W. Samuel, *Laser Photon. Rev.* **10**, 82–90 (2016).
- [8] K. Saxena, V. K. Jain, and D. S. Mehta, *Opt. Mater.* **32**, 221–233 (2009).
- [9] W. Brütting, J. Frischeisen, T. D. Schmidt, B. J. Scholz, and C. Mayr, *Phys. Status Solidi A* **210**, 44–65 (2013).
- [10] A. A. Erchak, D. J. Ripin, S. Fan, P. Rakich, J. D. Joannopoulos, E. P. Ippen, G. S. Petrich, and L. A. Kolodziejski, *Appl. Phys. Lett.* **78**, 563–565 (2001).
- [11] D.-H. Kim, C.-O. Cho, Y.-G. Roh, H. Jeon, and Y. S. Park, *Appl. Phys. Lett.* **87**(1–3), 203508 (2005).
- [12] J.-B. Kim, J.-H. Lee, C.-K. Moon, S.-Y. Kim, and J.-J. Kim, *Adv. Mater.* **25**, 3571–3577 (2013).
- [13] S. Möller and S. R. Forrest, *J. Appl. Phys.* **91**, 3324–3327 (2002).

- [14] J. Lim, S. S. Oh, D. Y. Kim, S. H. Cho, I. T. Kim, S. H. Han, H. Takezoe, E. H. Choi, G. S. Cho, Y. H. Seo, S. O. Kang, and B. Park, *Opt. Exp.* **14**, 6564–6571 (2006).
- [15] Y. F. Li, F. Li, J. H. Zhang, C. L. Wang, S. J. Zhu, H. J. Yu, Z. H. Wang, and B. Yang, *Appl. Phys. Lett.* **96**(1–3), 153305 (2010).
- [16] T. Yamasaki, K. Sumioka, and T. Tsutsui, *Appl. Phys. Lett.* **76**, 1243–1245 (2000).
- [17] F. Li, X. Li, J. H. Zhang, and B. Yang, *Org. Electron.* **8**, 635–639 (2007).
- [18] H. W. Chang, J. Lee, T. W. Koh, S. Hofmann, B. Lussem, S. Yoo, C. C. Wu, K. Leo, and M. C. Gather, *Laser Photon. Rev.* **7**, 1079–1087 (2013).
- [19] L. H. Smith and W. L. Barnes, *Org. Electron.* **7**, 490–494 (2006).
- [20] E. Kim, H. Cho, K. Kim, T. W. Koh, J. Chung, J. Lee, Y. K. Park and S. Yoo, *Adv. Mater.* **27**, 1624–1631 (2015).
- [21] T. W. Koh, J. A. Spechler, K. M. Lee, C. B. Arnold and B. P. Rand, *ACS Photon.* **2**, 1366–1372 (2015).
- [22] S. Mladenovski, K. Neyts, D. Pavicic, A. Werner and C. Rothe, *Opt. Express* **17**, 7562–7570 (2009).
- [23] T. Nakamura, H. Fujii, N. Juni and N. Tsutsumi, *Opt. Rev.* **13**, 104–110 (2006).
- [24] C. H. Chang, K. Y. Chang, Y. J. Lo, S. J. Chang, H. H. Chang, *Org. Electron.* **13**, 1073–1080 (2012).
- [25] D. Riedel, T. Wehler, T. C. G. Reusch, C. J. Brabec, *Org. Electron.* **32**, 27–33 (2016).
- [26] Y. Sun and S. R. Forrest, *Nature Photon.* **2**, 483–487 (2008).
- [27] M. Sliotzky and S. R. Forrest, *Opt. Lett.* **35**, 1052–1054 (2010).
- [28] Y. R. Do, Y. C. Kim, Y.-W. Song, C.-O. Cho, H. Jeon, Y.-J. Lee, S.-H. Kim, and Y.-H. Lee, *Adv. Mater.* **15**, 1214–1218 (2003).
- [29] Y.-J. Lee, S.-H. Kim, J. Huh, G.-H. Kim, Y.-H. Lee, S.-H. Cho, Y.-C. Kim, and Y. R. Do, *Appl. Phys. Lett.* **82**, 3779–3781 (2003).
- [30] M. Kitamura, S. Iwamoto, and Y. Arakawa, *Jpn. J. Appl. Phys.* **44**, 2844–2848 (2005).
- [31] Y. R. Do, Y.-C. Kim, Y.-W. Song, and Y.-H. Lee, *J. Appl. Phys.* **96**, 7629–7936 (2004).
- [32] S.-J. Park, Y. D. Kim, H. W. Lee, H. J. Yang, J.-Y. Cho, Y. K. Kim, and H. Lee, *Opt. Exp.* **22**, 12392–12397 (2014).
- [33] Y.-J. Lee, S.-H. Kim, G.-H. Kim, and Y.-H. Lee, *Opt. Exp.* **13**, 5864–5870 (2005).
- [34] L. Zschiedrich, H. J. Greiner, S. Burger, and F. Schmidt, *Conference on Light-Emitting Diodes-Materials, Devices, and Applications for Solid State Lighting*, **86410B**, (San Francisco, CA, 2013).
- [35] W. H. Koo, W. Youn, P. Zhu, X.-H. Li, N. Tansu, and F. So, *Adv. Funct. Mater.* **22**, 3454–3459 (2012).
- [36] C. S. Choi, S.-M. Lee, M. S. Lim, K. C. Choi, D. Kim, D. Y. Jeon, Y. Yang, and O. O. Park, *Opt. Exp.* **20**, A309–A318 (2012).
- [37] Y.-C. Kim and Y. R. Do, *Opt. Exp.* **13**, 1598–1603 (2005).
- [38] K. Hong, H. K. Yu, I. Lee, K. Kim, S. Kim, and J.-L. Lee, *Adv. Mater.* **22**, 4890–4894 (2010).
- [39] Z. Wang, Z. J. Chen, Z. H. Lan, X. F. Zhai, W. M. Du, and Q. H. Gong, *Appl. Phys. Lett.* **90**(1–3), 151119 (2007).
- [40] H. J. Peng, Y. L. Ho, X. J. Yu, and H. S. Kwok, *J. Appl. Phys.* **96**, 1649–1654 (2004).
- [41] W. H. Koo, S. M. Jeong, F. Araoka, K. Ishikawa, S. Nishimura, T. Toyooka, and H. Takezoe, *Nature Photon.* **4**, 222–226 (2010).
- [42] J.-W. Shin, D.-H. Cho, J. Moon, C. W. Joo, J. Lee, J. W. Huh, S. K. Park, J.-H. Han, N. S. Cho, J. Hwang, H. Y. Chu, and J.-I. Lee, *Opt. Lett.* **39**, 3527–3530 (2014).
- [43] H.-Y. Lin, J.-H. Lee, M.-K. Wei, C.-L. Dai, C.-F. Wu, Y.-H. Ho, H.-Y. Lin, and T.-C. Wu, *Opt. Commun.* **275**, 464–469 (2007).
- [44] J.-W. Shin, D.-H. Cho, J. Moon, C. W. Joo, S. K. Park, J. Lee, J.-H. Han, N. S. Cho, J. Hwang, J. W. Huh, H. Y. Chu, and J.-I. Lee, *Org. Electron.* **15**, 196–202 (2014).
- [45] W. H. Koo, S. M. Jeong, S. Nishimura, F. Araoka, K. Ishikawa, T. Toyooka, and H. Takezoe, *Adv. Mater.* **23**, 1003–1007 (2011).
- [46] B. J. Matterson, J. M. Lupton, A. F. Safonov, M. G. Salt, W. L. Barnes, and I. D. W. Samuel, *Adv. Mater.* **13**, 123–127 (2001).
- [47] P. A. Hobson, S. Wedge, J. A. E. Wasey, I. Sage, and W. L. Barnes, *Adv. Mater.* **14**, 1393–1396 (2002).
- [48] C. J. Yates, I. D. W. Samuel, P. L. Burn, S. Wedge, and W. L. Barnes, *Appl. Phys. Lett.* **88**(1–3), 161105 (2006).
- [49] H. A. Atwater, and A. Polman, *Nature Mater.* **9**, 205–213 (2010).
- [50] Q. Gan, F. J. Bartoli, and Z. H. Kafafi, *Adv. Mater.* **25**, 2385–2396 (2013).
- [51] J. Weickert, R. B. Dunbar, H. C. Hesse, W. Wiedemann, and L. S. Mende, *Adv. Mater.* **23**, 1810–1828 (2011).
- [52] Z. Tang, W. Tress and O. Inganäs, *Mater. Today* **17**, 389–396 (2014).
- [53] M. Wohlgenannt, K. Tandon, S. Mazumdar, S. Ramasesha, and Z. V. Vardeny, *Nature* **409**, 494–497 (2001).
- [54] L. C. Lin, H. F. Meng, J. T. Shy, S. F. Horng, L. S. Yu, C. H. Chen, H. H. Liaw, C. C. Huang, K. Y. Peng, and S. A. Chen, *Phys. Rev. Lett.* **90**(1–4), 036601 (2003).
- [55] J. S. Wilson, A. S. Dhoot, A. J. A. B. Seeley, M. S. Khan, A. Köhler, and R. H. Friend, *Nature* **413**, 828–831 (2001).
- [56] A. Köhler, J. S. Wilson, and R. H. Friend, *Adv. Mater.* **14**, 701–707 (2002).
- [57] L. Xiao, Z. J. Chen, B. Qu, J. X. Luo, S. Kong, Q. H. Gong, and J. J. Kido, *Adv. Mater.* **23**, 926–952 (2011).
- [58] L. X. Xiao, S.-J. Su, Y. Agata, H. Lan, and J. Kido, *Adv. Mater.* **21**, 1271–1274 (2009).
- [59] E. L. Williams, K. Haavisto, J. Li, and G. E. Jabbour, *Adv. Mater.* **19**, 197–202 (2007).
- [60] Q. Wang, J. Q. Ding, D. G. Ma, Y. X. Cheng, L. X. Wang, X. B. Jing, and F. S. Wang, *Adv. Funct. Mater.* **19**, 84–95 (2009).
- [61] F. B. Dias, K. N. Bourdakos, V. Jankus, K. C. Moss, K. T. Kamtekar, V. Bhalla, J. Santos, M. R. Bryce, and A. P. Monkman, *Adv. Mater.* **25**, 3707–3714 (2013).
- [62] H. Uoyama, K. Goushi, K. Shizu, H. Nomura, and C. Adachi, *Nature* **492**, 234–238 (2012).
- [63] S. Hirata, Y. Sakai, K. Masui, H. Tanaka, S. Y. Lee, H. Nomura, N. Nakamura, M. Yasumatsu, H. Nakanotani, Q. S. Zhang, K. Shizu, H. Miyazaki, and C. Adachi, *Nature Mater.* **14**, 330–336 (2015).
- [64] G. Gu, D. Z. Garbuzov, P. E. Burrows, S. Venkatesh, and S. R. Forrest, *Opt. Lett.* **22**, 396–398 (1997).

- [65] J. J. Shiang and A. R. Duggal, *J. Appl. Phys.* **95**, 2880–2888 (2004).
- [66] S.-Y. Kim and J.-J. Kim, *Org. Electron.* **11**, 1010–1015 (2010).
- [67] S. K. So, W. K. Choi, L. M. Leung, and K. Neyts, *Appl. Phys. Lett.* **74**, 1939–1941 (1999).
- [68] T. Tsutsui and K. Yamamoto, *Jpn. J. Appl. Phys.* **38**, 2799–2803 (1999).
- [69] M. H. Lu and J. C. Sturm, *Appl. Phys. Lett.* **78**, 1927–1929 (2001).
- [70] E. Ozbay, *Science* **311**, 189–193 (2006).
- [71] J. M. Pitarke, V. M. Silkin, E. V. Chulkov, and P. M. Echenique, *Rep. Prog. Phys.* **70**, 1–87 (2007).
- [72] H. Raether, *Surface Plasmons on Smooth and Rough Surfaces and on Gratings*.
- [73] W. L. Barnes, A. Dereux, and T. W. Ebbesen, *Nature* **424**, 824–830 (2003).
- [74] A. V. Zayatsa, I. I. Smolyaninov, and A. A. Maradudin, *Phys. Rep.* **408**, 131–314 (2005).
- [75] A. Giannattasio, S. Wedge, and W. L. Barnes, *J. Mod. Opt.* **53**, 429–436 (2006).
- [76] S. Y. Kim, W. I. Jeong, C. Mayr, Y. S. Park, K. H. Kim, J. H. Lee, C. K. Moon, W. Brütting and J. J. Kim, *Adv. Funct. Mater.* **23**, 3896–3900 (2013).
- [77] J. Frischeisen, D. Yokoyama, A. Endo, C. Adachi and W. Brütting, *Org. Electron.* **12**, 809–817 (2011).
- [78] C. Mayr, M. Taneda, C. Adachi and W. Brütting, *Org. Electron.* **15**, 3031–3037 (2014).
- [79] J. Y. Kim, T. Yasuda, Y. S. Yang and C. Adachi, *Adv. Mater.* **25**, 2666–2671 (2013).
- [80] C. Mayr, S. Y. Lee, T. D. Schmidt, T. Yasuda, C. Adachi and W. Brütting, *Adv. Funct. Mater.* **24**, 5232–5239 (2014).
- [81] D. Yokoyama, Y. Setoguchi, A. Sakaguchi, M. Suzuki and C. Adachi, *Adv. Funct. Mater.* **20**, 386–391 (2010).
- [82] G. Gu, V. Bulović, P. E. Burrows, S. R. Forrest, and M. E. Thompson, *Appl. Phys. Lett.* **68**, 2606–2608 (1996).
- [83] P. Görrn, M. Sander, J. Meyer, M. Kröger, E. Becker, H.-H. Johannes, W. Kowalsky, and T. Riedl, *Adv. Mater.* **18**, 738–741 (2006).
- [84] J. Meyer, T. Winkler, S. Hamwi, S. Schmale, H.-H. Johannes, T. Weimann, P. Hinze, W. Kowalsky, and T. Riedl, *Adv. Mater.* **20**, 3839–3843 (2008).
- [85] P. Kuang, J.-M. Park, W. Leung, R. C. Mahadevapapuram, K. S. Nalwa, T.-G. Kim, S. Chaudhary, K.-M. Ho, and K. Constant, *Adv. Mater.* **23**, 2469–2473 (2011).
- [86] M. G. Helander, Z.-B. Wang, M. T. Greiner, Z.-W. Liu, J. Qiu, and Z.-H. Lu, *Adv. Mater.* **22**, 2037–2040 (2010).
- [87] S. M. Jeong and H. Takezoe, *InTech Chapter 4*, 66–104 (2012).
- [88] J. Henson, J. DiMaria, and R. Paiella, *J. Appl. Phys.* **106**(1–6), 093111 (2009).
- [89] E. Popov, N. Bonod, and S. Enoch, *Opt. Exp.* **15**, 4224–4237 (2007).
- [90] D. K. Gifford and D. G. Hall, *Appl. Phys. Lett.* **81**, 4315–4317 (2002).
- [91] M. Fujita, T. Ueno, K. Ishihara, T. Asano, S. Nodab, H. Ohata, T. Tsuji, and H. Nakada, *Appl. Phys. Lett.* **85**, 5769–5771 (2004).
- [92] J. Feng and T. Okamoto, *Opt. Lett.* **30**, 2302–2304 (2005).
- [93] J. Feng, T. Okamoto, and S. Kawata, *Appl. Phys. Lett.* **87**(1–3), 241109 (2005).
- [94] J. Feng, T. Okamoto, J. Simonen, and S. Kawata, *Appl. Phys. Lett.* **90**(1–3), 081106 (2007).
- [95] J. Feng, T. Okamoto, R. Naraoka, and S. Kawata, *Appl. Phys. Lett.* **93**(1–3), 051106 (2008).
- [96] Y. Jin, J. Feng, X.-L. Zhang, Y.-G. Bi, Y. Bai, L. Chen, T. Lan, Y.-F. Liu, Q.-D. Chen, and H.-B. Sun, *Adv. Mater.* **24**, 1187–1191 (2012).
- [97] S. Jeon, J.-H. Lee, J.-H. Jeong, Y. S. Song, C.-K. Moon, J.-J. Kim, and J. R. Youn, *Sci. Rep.* **5**(1–7), 8685 (2015).
- [98] D. Y. Kim, S. K. Tripathy, L. Li, and J. Kumar, *Appl. Phys. Lett.* **66**, 1166–1168 (1995).
- [99] T. Lippert, T. Gerber, A. Wokaun, D. J. Funk, H. Fukumura, and M. Goto, *Appl. Phys. Lett.* **75**, 1018–1020 (1999).
- [100] F. Yu, P. Li, H. Shen, S. Mathur, C. M. Lehr, U. Bakowsky, and F. Mücklich, *Biomaterials* **26**, 2307–2312 (2005).
- [101] Y. Bai, J. Feng, Y.-F. Liu, J.-F. Song, J. Simonen, Y. Jin, Q.-D. Chen, J. Zi, and H.-B. Sun, *Org. Electron.* **12**, 1927–1935 (2011).
- [102] A. O. Altun, S. Jeon, J. Shim, J.-H. Jeong, D.-G. Choi, K.-D. Kim, J.-H. Choi, S.-W. Lee, E.-S. Lee, H.-D. Park, J. R. Youn, J.-J. Kim, Y.-H. Lee, and J.-W. Kang, *Org. Electron.* **11**, 711–716 (2010).
- [103] E. Kint, Y. Xict, X.-M. Zhao, and G. M. Whitesides, *Adv. Mater.* **9**, 651–654 (1997).
- [104] Y. X. Lu, X. L. Chen, W. Hu, N. Lu, J. Q. Sun, and J. C. Shen, *Langmuir* **23**, 3254–3259 (2007).
- [105] V. Reboud, A. Z. Khokhar, B. Sepúlveda, D. Dudek, T. Kehoe, J. Cuffe, N. Kehagias, M. Lira-Cantu, N. Gadegaard, V. Grasso, V. Lambertini, and C. M. S. Torres, *Nanoscale* **4**, 3495–3500 (2012).
- [106] J. Wang, X. Y. Sun, L. Chen, and S. Y. Chou, *Appl. Phys. Lett.* **75**, 2767–2769 (1999).
- [107] J. R. Lawrence, G. A. Turnbull, and I. D. W. Samuel, *Appl. Phys. Lett.* **82**, 4023–4025 (2003).
- [108] F. Galeotti, W. Mróz, G. Scavia, and C. Botta, *Org. Electron.* **14**, 212–218 (2013).
- [109] H.-J. Peng, Y. L. Ho, X.-J. Yu, M. Wong, and H.-S. Kwok, *J. Disp. Tech.* **1**, 278–282 (2005).
- [110] J.-M. Park, Z. Q. Gan, W. Y. Leung, R. Liu, Z. Ye, K. Constant, J. Shinar, R. Shinar, and K.-M. Ho, *Opt. Exp.* **19**, A786–A792 (2011).
- [111] T. Höfler, M. Weinberger, W. Kern, S. Rentenberger, and A. Pogantsch, *Adv. Funct. Mater.* **16**, 2369–2373 (2006).
- [112] D.-Y. Kim, C. S. Choi, J. Y. Kim, D. H. Kim, and K. C. Choi, *Org. Electron.* **15**, 1222–1228 (2014).
- [113] X.-B. Shi, M. Qian, Z.-K. Wang, and L.-S. Liao, *Appl. Phys. Lett.* **106**(1–4), 223301 (2015).
- [114] R. F. Garcia, L. Zeng, S. Khadir, M. Chakaroun, A. P. A. Fischer and A. Boudrioua, *J. Opt. Soc. Am. B* **33**, 246–252 (2016).
- [115] N. F. Chiu, C. H. Hou, C. J. Cheng and F. Y. Tsai, *Int. J. Photoenergy* **2013**, 502576 (2013).
- [116] N. C. Lindquist, W. A. Luhman, S. H. Oh and R. J. Holmes, *Appl. Phys. Lett.* **93**, 123308 (2008).
- [117] M. C. Gather, A. Köhnen, A. Falcou, H. Becker and K. Meerholz, *Adv. Funct. Mater.* **17**, 191–200 (2007).

- [118] M. Jung, D. M. Yoon, M. Kim, C. Kim, T. Lee, J. H. Kim, S. Lee, S.-H. Lim, and D. Woo, *Appl. Phys. Lett.* **105**(1–5), 013306 (2014).
- [119] K. Endo and C. Adachi, *Appl. Phys. Lett.* **104**(1–4), 121102 (2014).
- [120] S. Moller and S. R. Forrest, *J. Appl. Phys.* **91**, 3324–3327 (2002).
- [121] Y. Sun and S. R. Forrest, *J. Appl. Phys.* **100**(1–6), 073106 (2006).
- [122] J. P. Yang, Q. Y. Bao, Z. Q. Xu, Y. Q. Li, J. X. Tang, and S. Shen, *Appl. Phys. Lett.* **97**(1–3), 223303 (2010).
- [123] S.-H. Eom, E. Wrzesniewski, and J. Xue, *Org. Electron.* **12**, 472–476 (2011).
- [124] M. Thomschke, S. Reineke, B. Lüssem, and K. Leo, *Nano Lett.* **12**, 424–428 (2012).
- [125] J. H. Lee, Y. H. Ho, K. Y. Chen, H. Y. Lin, J. H. Fang, S. C. Hsu, J. R. Lin, and M. K. Wei, *Opt. Exp.* **16**, 21184–21190 (2008).
- [126] X. X. Fu, X. N. Kang, B. Zhang, C. Xiong, X. Z. Jiang, D. S. Xu, W. M. Du, and G. Y. Zhang, *J. Mater. Chem.* **21**, 9576–9581 (2011).
- [127] S. Reineke, F. Lindner, G. Schwartz, N. Seidler, K. Walzer, B. Lussem, and K. Leo, *Nature* **459**, 234–238 (2009).
- [128] J. S. Lin, S. H. Lin, N. P. Chen, C. H. Ko, Z. S. Tsai, F. S. Juang, C. M. Chen, and L. C. Liu, *Synth. Met.* **160**, 1493–1500 (2010).
- [129] R. Bathelt, D. Buchhauser, C. Gärditz, R. Paetzold, and P. Wellmann, *Org. Electron.* **8**, 293–297 (2007).
- [130] S. W. Liu, J. X. Wang, Y. Divayana, K. Dev, S. T. Tan, H. V. Demir, and X. W. Sun, *Appl. Phys. Lett.* **102**(1–4), 053305 (2013).
- [131] D. K. Gifford and D. G. Hall, *Appl. Phys. Lett.* **80**, 3679–3681 (2002).
- [132] T. Okamoto and K. Shinotsuka, *Appl. Phys. Lett.* **104**(1–4), 093301 (2014).
- [133] X.-L. Zhang, J.-F. Song, J. Feng, and H.-B. Sun, *Opt. Lett.* **38**, 4382–4385 (2013).
- [134] P. T. Worthing and W. L. Barnes, *Appl. Phys. Lett.* **79**, 3035–3037 (2001).
- [135] W. Youn, J. Lee, M. Xu, R. Singh, and F. So, *ACS Appl. Mater. Interfaces* **7**, 8974–8978 (2015).
- [136] S.-M. Lee, J.-S. Chae, D.-Y. Kim, and K. C. Choi, *Org. Electron.* **15**, 3354–3361 (2014).
- [137] Y.-G. Bi, J. Feng, Y.-F. Li, Y. Jin, Y.-F. Liu, Q.-D. Chen, and H.-B. Sun, *Appl. Phys. Lett.* **100**(1–4), 053304 (2012).
- [138] J.-W. Park, G.-H. Lee, Y. Y. Kwon, K.-W. Park, J. Lee, Y. W. Jin, Y.-C. Nah, and H. Kim, *Org. Electron.* **15**, 2178–2183 (2014).
- [139] Y.-G. Bi, J. Feng, Y.-F. Li, X.-L. Zhang, Y.-F. Liu, Y. Jin, and H.-B. Sun, *Adv. Mater.* **25**, 6969–6974 (2013).
- [140] S. J. Shin, T. H. Park, J. H. Choi, E. H. Song, H. Kim, H. J. Lee, J.-I. Lee, H. Y. Chu, K. B. Lee, Y. W. Park, and B.-K. Ju, *Org. Electron.* **14**, 187–192 (2013).
- [141] T. Bocksrocker, J. Hoffmann, C. Eschenbaum, A. Pargner, J. Preinfalk, F. Maier-Flaig, and U. Lemmer, *Org. Electron.* **14**, 396–401 (2013).
- [142] J. Y. Kim, W. H. Kim, D. H. Kim, and K. C. Choi, *Org. Electron.* **15**, 260–265 (2014).
- [143] J. Moona, E. Kim, S. K. Park, K. Lee, J.-W. Shin, D.-H. Cho, J. Lee, C. W. Joo, N. S. Cho, J.-H. Han, B.-G. Yu, S. Yoo, and J.-I. Lee, *Org. Electron.* **26**, 273–278 (2015).
- [144] W. H. Koo, S. Y. Boo, S. M. Jeong, S. Nishimura, F. Araoka, K. Ishikawa, T. Toyooka, and H. Takezoe, *Org. Electron.* **12**, 1177–1183 (2011).
- [145] Y. H. Kim, J. Lee, W. M. Kim, C. Fuchs, S. Hofmann, H.-W. Chang, M. C. Gather, L. Müller-Meskamp, and K. Leo, *Adv. Funct. Mater.* **24**, 2553–2559 (2014).
- [146] M. Heo, H. Cho, J.-W. Jung, J.-R. Jeong, S. Park, and J. Y. Kim, *Adv. Mater.* **23**, 5689–5693 (2011).
- [147] S. H. Kim, T.-S. Bae, W. Heo, T. Joo, K.-D. Song, H.-G. Park, and S. Y. Ryu, *ACS Appl. Mater. Interfaces* **7**, 15031–15041 (2015).
- [148] B. Riedel, J. Hauss, U. Geyer, J. Guetlein, U. Lemmer, and M. Gerken, *Appl. Phys. Lett.* **96**(1–3), 243302 (2010).
- [149] Y. Xiao, J. P. Yang, P. P. Cheng, J. J. Zhu, Z. Q. Xu, Y. H. Deng, S. T. Lee, Y. Q. Li, and J. X. Tang, *Appl. Phys. Lett.* **100**(1–4), 013308 (2012).
- [150] A. Kumar, R. Srivastava, P. Tyagi, D. S. Mehta, and M. N. Kamalasanan, *Org. Electron.* **13**, 159–165 (2012).
- [151] H. Sung, J. Lee, K. Han, J.-K. Lee, J. Sung, D. Kim, M. Choi, and C. Kim, *Org. Electron.* **15**, 491–499 (2014).
- [152] D.-D. Zhang, R. Wang, Y.-Y. Ma, H.-X. Wei, Q.-D. Ou, Q.-K. Wang, L. Zhou, S.-T. Lee, Y.-Q. Li, and J.-X. Tang, *Org. Electron.* **15**, 961–967 (2014).
- [153] W. Y. Ji, H. F. Zhao, H. G. Yang, and F. R. Zhu, *Org. Electron.* **22**, 154–159 (2015).
- [154] Q.-D. Ou, L. Zhou, Y.-Q. Li, S. Shen, J.-D. Chen, C. Li, Q.-K. Wang, S.-T. Lee, and J.-X. Tang, *Adv. Funct. Mater.* **24**, 7249–7256 (2014).
- [155] L. Zhou, Q.-D. Ou, Y.-Q. Li, H.-Y. Xiang, L.-H. Xu, J.-D. Chen, C. Li, S. Shen, S.-T. Lee, and J.-X. Tang, *Adv. Funct. Mater.* **25**, 2660–2668 (2015).
- [156] Y. S. Shim, J. H. Hwang, H. J. Lee, K. B. Choi, K. N. Kim, C. H. Park, S.-G. Jung, Y. W. Park, and B.-K. Ju, *Adv. Funct. Mater.* **24**, 6414–6421 (2014).
- [157] W. Ding, Y. X. Wang, H. Chen, and S. Y. Chou, *Adv. Funct. Mater.* **24**, 6329–6339 (2014).
- [158] H.-Y. Xiang, Y.-Q. Li, L. Zhou, H.-J. Xie, C. Li, Q.-D. Ou, L.-S. Chen, C.-S. Lee, S.-T. Lee, and J.-X. Tang, *ACS NANO* **9**, 7553–7562 (2015).
- [159] L. Li, J. J. Liang, S.-Y. Chou, X. D. Zhu, X. F. Niu, Z. B. Yu, and Q. B. Pei, *Sci. Rep.* **4**(1–8), 4307 (2014).
- [160] R. H. Jordan, A. Dodabalapur, and R. E. Slusher, *Appl. Phys. Lett.* **69**, 1997 (1996).
- [161] M. Agrawal, Y. Sun, S. R. Forrest and P. Peumans, *Appl. Phys. Lett.* **90**, 241112 (2007).
- [162] S. Chen, L. Deng, J. Xie, L. Peng, L. Xie, Q. Fan, and W. Huang, *Adv. Mater.* **22**, 5227–5239 (2010).
- [163] S. Hofmann, M. Thomschke, B. Lüssem, and K. Leo, *Opt. Exp.* **19**, A1250–A1264 (2011).
- [164] M. Thomschke, R. Nitsche, M. Furno, and K. Leo, *Appl. Phys. Lett.* **94**, 083303 (2009).
- [165] P. Freitag, S. Reineke, S. Olthof, M. Furno, B. Lüssem, and K. Leo, *Org. Electron.* **11**, 1676–1682 (2010).
- [166] T. Schwab, S. Schubert, L. Müller-Meskamp, K. Leo, and M. C. Gather, *Adv. Opt. Mater.* **1**, 921–925 (2013).
- [167] W. Ji, L. Zhang, T. Zhang, G. Liu, W. Xie, S. Liu, H. Zhang, L. Zhang, and B. Li, *Opt. Lett.* **34**, 2703–2705 (2009).

- [168] D. S. Leem, S. Y. Kim, J. H. Lee and J. J. Kim, *J. Appl. Phys.* **106**, 063114 (2009).
- [169] C.-J. Yang, S.-H. Liu, H.-H. Hsieh, C.-C. Liu, T.-Y. Cho, and C.-C. Wua, *Appl. Phys. Lett.* **91**(1–3), 253508 (2007).
- [170] E. Wrzesniewski, S.-H. Eom, W. Cao, W. T. Hammond, S. Lee, E. P. Douglas, and J. Xue, *Small* **8**, 2647–2651 (2012).
- [171] X.-L. Zhang, J. Feng, X.-C. Han, Y.-F. Liu, Q.-D. Chen, J.-F. Song, and H.-B. Sun, *Optica* **2**, 579–584 (2015).
- [172] Y.-F. Liu, J. Feng, D. Yin, H.-F. Cui, X.-L. Zhang, Y.-G. Bi, D.-D. Zhang, L.-S. Liu, A.-W. Li, J.-F. Song, Q.-D. Chen, and H.-B. Sun, *Org. Electron.* **14**, 1597–1601 (2013).
- [173] Y.-F. Liu, J. Feng, Y.-G. Bi, J.-F. Song, Y. Jin, Y. Bai, Q.-D. Chen, and H.-B. Sun, *Opt. Lett.* **37**, 124–126 (2012).
- [174] J. W. Huh, J.-W. Shin, D.-H. Cho, J. Moon, C. W. Joo, S. K. Park, J. Hwang, N. S. Cho, J. Lee, J.-H. Han, H. Y. Chu, and J.-I. Lee, *Nanoscale* **6**, 10727–10733 (2014).
- [175] W. H. Weber and C. F. Eagen, *Opt. Lett.* **4**, 236–238 (1979).
- [176] K. Y. Yang, K. C. Choi, and C. W. Ahn, *Opt. Exp.* **17**, 11495–11504 (2009).
- [177] T. Nakamura, M. Fujii, K. Imakita, and S. Hayashi, *Phys. Rev. B* **72**(1–6), 235412 (2005).
- [178] T. Tsutsui, N. Takada, S. Saito, and E. Ogino, *Appl. Phys. Lett.* **65**, 1868–1870 (1994).
- [179] J.-J. Greffet, R. Carminati, K. Joulain, J.-P. Mulet, S. Mainguy, and Y. Chen, *Nature*, **416**, 61–64 (2002).
- [180] D. Z. Lin, C. K. Chang, Y. C. Chen, D. L. Yang, M. W. Lin, J. T. Yeh, J. M. Liu, C. H. Kuan, C. S. Yeh, and C. K. Lee, *Opt. Exp.* **14**, 3503–3511 (2006).
- [181] L. Martín-Moreno, F. J. García-Vidal, H. J. Lezec, A. Degiron, and T. W. Ebbesen, *Phys. Rev. Lett.* **90**(1–4), 167401 (2003).
- [182] H. J. Lezec, A. Degiron, E. Devaux, R. A. Linke, L. Martín-Moreno, F. J. García-Vidal, and T. W. Ebbesen, *Science* **297**, 820–822 (2002).
- [183] P. Andrew and W. L. Barnes, *Science* **306**, 1002–1005 (2004).
- [184] Y. Jin, J. Feng, X.-L. Zhang, M. Xu, Q.-D. Chen, Z.-J. Wu, and H.-B. Sun, *Appl. Phys. Lett.* **106**(1–5), 223303 (2015).
- [185] P. W. M. Blom, V. D. Mihailetschi, L. J. A. Koster, and D. E. Markov, *Adv. Mater.* **19**, 1551–1566 (2007).
- [186] L. M. Chen, Z. Hong, G. Li, and Y. Yang, *Adv. Mater.* **21**, 1434–1449 (2009).
- [187] M. Xu, J. Feng, Y. S. Liu, Y. Jin, H. Y. Wang, and H. B. Sun, *Appl. Phys. Lett.* **105**, 153303 (2014).
- [188] A. J. Morfa, K. L. Rowlen, T. H. Reilly III, M. J. Romero, and J. Lagemaat, *Appl. Phys. Lett.* **92**, 013504 (2008).
- [189] S. Soon Kim, S. I. Na, J. Jo, D. Y. Kim, and Y. C. Nah, *Appl. Phys. Lett.* **93**, 073307 (2008).
- [190] Y. Jin, J. Feng, X. L. Zhang, M. Xu, Y. G. Bi, Q. D. Chen, H. Y. Wang, and H. B. Sun, *Appl. Phys. Lett.* **101**, 163303 (2012).
- [191] Y. Jin, J. Feng, Y. H. Wang, M. Xu, T. Lan, Y. G. Bi, Q. D. Chen, H. Y. Wang, and H. B. Sun, *IEEE Photon. J.* **4**, 1737–1743 (2012).
- [192] Y. Jin, J. Feng, M. Xu, X. L. Zhang, L. Wang, Q. D. Chen, H. Y. Wang, and H. B. Sun, *Adv. Optical Mater.* **1**, 809–813 (2013).
- [193] M. G. Kang, T. Xu, H. J. Park, X. Luo, and L. J. Guo, *Adv. Mater.* **22**, 4378–4383 (2010).
- [194] C. Min, J. Li, G. Veronis, J. Y. Lee, S. Fan, and P. Peumans, *Appl. Phys. Lett.* **96**, 133302 (2010).
- [195] H. W. Chang, J. Lee, S. Hofmann, Y. H. Kim, L. M. Meskamp, B. Lüssem, C. C. Wu, K. Leo and M. C. Gather, *J. Appl. Phys.* **113**, 204502 (2013).
- [196] J. Xiong, B. Yang, J. Yuan, L. Fan, X. Hu, H. Xie, L. L. Yu, R. Cui, Y. Zou, C. Zhou, D. Niu, Y. Gao and J. Yang, *Org. Electron.* **17**, 253–261 (2015).
- [197] Y. Park, L. M. Meskamp, K. Vandewal and K. Leo, *Appl. Phys. Lett.* **108**, 253302 (2016).
- [198] H. A. Atwater and A. Polman, *Nat. Mater.* **9**, 205–213 (2010).
- [199] Q. Gan, F. J. Bartoli and Z. H. Kafafi, *Adv. Mater.* **25**, 2385–2396 (2013).
- [200] S. I. Na, S. S. Kim, J. Jo, S. H. Oh, J. Kim, and D. Y. Kim, *Adv. Funct. Mater.* **18**, 3956–3963 (2008).
- [201] M. A. M. Teridi, M. Sookhakian, W. J. Basirun, R. Zakaria, F. K. Schneider, W. J. d. Silva, J. Kim, S. J. Lee, H. P. Kim, A. R. b. M. Yusoff and J. Jang, *Nanoscale*, **7**, 7091–7100 (2015).
- [202] A. K. Pandey, M. Aljada, M. Velusamy, P. L. Burn, and P. Meredith, *Adv. Mater.* **24**, 1055–1061 (2012).
- [203] D. H. Ko, J. R. Tumbleston, L. Zhang, S. Williams, J. M. DeSimone, R. Lopez, and E. T. Samulski, *Nano Lett.* **9**, 2742–2746 (2009).
- [204] J. W. Leem, S. Kim, S. H. Lee, J. A. Rogers, E. Kim, and J. S. Yu, *Adv. Energy Mater.* **4**, 1301315 (2014).
- [205] L. M. Meskamp, Y. H. Kim, T. Roch, S. Hofmann, R. Scholz, S. Eckardt, K. Leo, and A. F. Lasagni, *Adv. Mater.* **24**, 906–910 (2012).
- [206] J. D. Chen, L. Zhou, Q. D. Ou, Y. Q. Li, S. Shen, S. T. Lee, and J. X. Tang, *Adv. Energy Mater.* **4**, 1301777 (2014).
- [207] X. Li, W. C. H. Choy, L. Huo, F. Xie, W. E. I. Sha, B. Ding, X. Guo, Y. Li, J. Hou, J. You, and Y. Yang, *Adv. Mater.* **24**, 3046–3052 (2012).
- [208] X. Li, X. Ren, F. Xie, Y. Zhang, T. Xu, B. Wei, and W. C. H. Choy, *Adv. Optical Mater.* **3**, 1220–1231 (2015).
- [209] A. S. Hall, M. Faryad, G. D. Barber, L. Liu, S. Erten, T. S. Mayer, A. Lakhtakia, and T. E. Mallouk, *ACS Nano* **7**, 4995–5007 (2013).
- [210] Y. G. Bi, J. Feng, Y. Chen, Y. S. Liu, X. L. Zhang, Y. F. Li, M. Xu, Y. F. Liu, X. C. Han, H. B. Sun, *Org. Electron.* **27**, 167–172 (2015).
- [211] J. D. Chen, C. Cui, Y. Q. Li, L. Zhou, Q. D. Ou, C. Li, Y. Li, and J. X. Tang, *Adv. Mater.* **27**, 1035–1041 (2015).
- [212] J. Ham, W. J. Dong, J. Y. Park, C. J. Yoo, I. Lee, and J. L. Lee, *Adv. Mater.* **27**, 4027–4033 (2015).
- [213] H. Kwon, J. Ham, D. Y. Kim, S. J. Oh, S. Lee, S. H. Oh, E. F. Schubert, K. G. Lim, T. W. Lee, S. Kim, J. L. Lee, and J. K. Kim, *Adv. Energy Mater.* **4**, 1301566 (2014).